ρ 44

CONTROL & REDUCTION OF UNSTEADY PRESSURE LOADS IN SEPARATED SHOCK WAVE TURBULENT BOUNDARY LAYER INTERACTION

David S. Dolling and J. W. Barter

CENTER FOR AEROMECHANICS RESEARCH
Department of Aerospace Engineering & Engineering Mechanics
The University of Texas at Austin
Austin, Texas 78712

August 1995

CONTENTS

General Introduction and Explanation of Report Layout

Publication of Results

Section 1: Experimental Study of the Use of Vortex Generators to Reduce Fluctuating Pressure Loads in Shock Wave Turbulent Boundary Layer Interactions

Section 2: Reduction of Fluctuating Pressure Loads in Shock Wave Turbulent Boundary Layer Interactions

General Introduction and Explanation of Report Layout

The focus of the experimental work carried out under NASA Research Grant NAG 1-1471 was on developing means of controlling and reducing unsteady pressure loads in separated shock wave turbulent boundary layer interactions. Due to budget constraints, funding was terminated before completion of the project, and thus all of the work planned under the original proposal could not be carried out. Nevertheless, part of the planned work was completed and provided promising results. These studies are described in detail in Sections 1 and 2 of the report. Section 1 describes how vortex generators can be used to effectively reduce loads in compression ramp interaction, while Section 2 focuses on the effects of "boundary-layer separators" on the same interaction. Both of these studies have been presented at national AIAA Technical Conferences, and papers describing the vortex generator studies have been accepted for publication in the *AIAA Journal.*

Publication of Results

Conference Presentations

Barter, J. W., and Dolling, D. S., "Experimental Study of Use of Vortex Generators to Reduce Fluctuation Pressure Loads in Shock Wave Turbulent Boundary Layer Interactions," AIAA Paper 93-4335, 15th Aeroacoustics Conference, Long Beach, CA, Oct. 25–27, 1993.

Barter, J. W., and Dolling, D. S., "Reduction of Fluctuating Pressure Loads in Shock Wave Turbulent Boundary Layer Interactions," AIAA Paper 95-0673, AIAA 33rd Aerospace Sciences Meeting, Reno, NV, Jan. 9–12, 1995.

Refereed Journal Articles

Barter, J. W., and Dolling, D. S., "Reduction of Fluctuating Pressure Loads in Shock Wave Turbulent Boundary Layer Interactions Using Vortex Generators," accepted for publication by *AIAA Journal*, 1995.

Barter, J. W., and Dolling, D. S., "Reduction of Fluctuation Pressure Loads in Shock Wave Boundary Layer Interactions Using Vortex Generators II," accepted for publication by *AIAA Journal*, 1995.

Section 1:

Experimental Study of the Use of Vortex Generators to Reduce Fluctuating Pressure Loads in Shock Wave Turbulent Boundary Layer Interactions

Experimental Study of the Use of Vortex Generators to Reduce Fluctuating Pressure Loads in Shock Wave Turbulent Boundary Layer Interactions

J. W. Barter[*] and D. S. Dolling[+]

Fluctuating wall pressure measurements have been made in a separated shock wave/turbulent boundary layer interaction produced by an unswept compression corner in a Mach 5 flow. Wheeler doublet vortex generators were placed 15.8 boundary layer thicknesses upstream of the corner to study their effect on the fluctuating pressure loads produced by the translating separation shock. The vortex generators produced significant three-dimensionality in an otherwise two-dimensional interaction. They reduced the upstream influence and the length of the region of shock motion by 60% and 64%, respectively, decreased the maximum wall pressure RMS by 23%, and shifted the fluctuations to a higher frequency band. The maximum fraction of energy in the 100-500 Hz frequency band is decreased by 11%. These changes are due to a fuller boundary layer profile, a weaker separation shock, and increased boundary layer turbulence causing increased separation shock jitter.

Nomenclature

C_f skin friction coefficient
$G(f)$ spectral density function
L_i intermittent region length
N number of separation shock crossings
P pressure
Re_δ Reynolds number based on boundary layer thickness
T temperature, separation shock period
U velocity
X streamwise distance nondimensionalized by δ (fig. 1)
Y spanwise distance nondimensionalized by δ (fig. 1)
Z vertical distance nondimensionalized by δ (fig. 1)
f frequency
f_c separation shock zero crossing frequency
t_f fall time (eq. 1)
t_r rise time (eq. 1)
Π undisturbed boundary layer wake strength parameter
β fraction of wall pressure variance in the 100-500 Hz. band
δ undisturbed boundary layer thickness
δ^* undisturbed boundary layer displacement thickness
γ wall pressure signal intermittency
σ standard deviation
θ undisturbed boundary layer momentum thickness

---

[*] Graduate Student, Student Member AIAA
[+] Professor, Associate Fellow AIAA

Subscripts:
0   boundary layer
(̄)   average quantity
max   maximum value
o   stagnation quantity
pw   wall pressure
rms   root mean square value
t   pitot pressure
vg   vortex generator
w   wall
∞,inf freestream condition

Abbreviations:
PDF   probability density function
S   separation line
SWTBLI   shock wave/turbulent boundary layer interaction
UI   upstream influence line
VG   vortex generator

Introduction

It is well known that when a shock wave of sufficient strength interacts with a boundary layer it can cause separation. In the case of shock-induced turbulent boundary layer separation, high speed cinematography as early as the 1950's[1,2] showed that the process is unsteady. However, due to the lack of adequate instrumentation, most early studies addressed mean flow properties only. Kistler,[3] in 1964, was probably the first to make detailed fluctuating wall pressure measurements under the separated supersonic turbulent boundary layer upstream of a forward facing step. Since Kistler, there has been an increasing number of studies focusing on interaction unsteadiness. The qualitative character and quantitative details of the unsteadiness naturally vary from one flow type to another, but typically the unsteadiness manifests itself as a large-scale, low-frequency pulsation of the separated flow and flapping of the outgoing boundary layer. A recent review of much of this work has been compiled by Dolling.[4]

Interaction unsteadiness produces large amplitude fluctuating pressure loads as high as 185 dB which can substantially shorten the fatigue life of vehicle components. These high loads occur near separation and reattachment, and under the outgoing boundary layer, and are caused by fluctuations in the instantaneous positions of separation and reattachment. The frequency band of the highest amplitude loads is typically in the range of several hundred Hz to several kHz. This band exacerbates the loading problem because the typical resonant frequency band for skin panels is 100-500 Hz. Predictions by Pozefsky, et al.[5] for a transatmospheric vehicle suggest that the time to failure of conventional structures under such loading is typically of order minutes.

The region of separated flow produced by shock wave turbulent boundary layer interactions can also substantially reduce aerodynamic efficiency. Consequently, many previous attempts to control these interactions have focused on either eliminating separation or reducing the total pressure loss through the shock.[6-10] In light of the effect of shock wave turbulent boundary layer interactions on structural fatigue, some recent control studies have focused on loads reduction. McClure[11] explored a number of techniques, including LEBUs and riblets, with limited success. Kleifges and Dolling[12] had greater success using a swept root fillet to reduce the loads produced in an unswept blunt fin induced interaction.

The objective of the current study is to explore ways to reduce fluctuating pressure loads in shock wave turbulent boundary layer interactions in order to extend fatigue life. It is hoped that through changes in the separation shock dynamics (and reattachment process), the magnitude of the loading can be reduced, its spectral content altered, and the area exposed to high loads reduced. In the exploratory study reported in this paper, the effects of Wheeler doublet vortex generators[13] are examined.

Previous experiments have shown vane-type vortex generators (VGs) are ineffective in controlling shock-induced turbulent boundary layer separation.[14] Wheeler doublets are better suited for this application because they produce a relatively benign shock pattern as compared to that produced by

vane-type VGs. The Wheeler doublets, unlike vane VGs, do not produce shocks which impinge on the shock wave turbulent boundary layer interaction. Each Wheeler doublet produces a pair of counter-rotating vortices which energize the boundary layer by transferring high momentum fluid from the outer region of the boundary layer to the inner region. Low momentum fluid swept from under the vortices collects between the counter-rotating pair.[15] In the case of the Wheeler doublets, this produces a relatively low-momentum region downstream of the VG apexes. Barber, et al.[16] conducted a computational, parametric study of Wheeler doublets to determine the geometry that best energizes the boundary layer. Of the configurations tested, their results indicate that a length:width:height ratio of 6:5:1 is best.

The motivation for this study stems from observations made in previous studies. McCormick[17] placed Wheeler doublets upstream of a normal shock/turbulent boundary layer interaction. Although only mean pressure measurements were made, it appeared from McCormick's results that the intermittent region (i.e., the region of separation shock motion) was shorter as compared to the undisturbed interaction. This inference is based on observations from other studies which have shown that the intermittent region spans the region from the upstream influence line to the separation line (as determined from the mean pressure distribution and surface tracer patterns). Gonsalez and Dolling[18] have also observed that in a given boundary layer the separation shock velocities are independent of the intermittent region length, and thus with a smaller intermittent region, shock frequencies increase. These two observations suggested that the placement of Wheeler doublets upstream of an interaction would shift separation shock motion to a higher frequency band through shortening of the intermittent region. This in turn shifts the fluctuating pressure loads to a higher frequency band.

This paper presents the first set of results from an ongoing study. Herein the effects of the Wheeler doublets on the intermittent region of an unswept compression corner induced interaction are addressed. Later phases of this study will focus on the effect of the doublets on the ramp face loading and flowfield.

Experimental Program

Wind Tunnel and Flow Conditions

All experiments were conducted in the Mach 5 blowdown wind tunnel at The University of Texas at Austin. The air supply for this tunnel is stored in tanks with a combined volume of 140 ft.^{3} (3.96 m^3) at a maximum pressure of 2500 psig. (17.3 MPa). Maximum run times are about a minute. A computer controlled valve regulates the flow of air from the tanks to the settling chamber such that a constant stagnation pressure (to within ±1.5%) is maintained. Two banks of 420 kW nichrome wire heaters raise the temperature of the air in the settling chamber to the desired value.

The test section used for these experiments is 27 in. (68.6 cm) long, 6 in. (15.2 cm) wide and 7 in. (17.8 cm) high. All tests were conducted with the models mounted on the test section floor. The floor boundary layer undergoes natural transition upstream of the nozzle and develops under approximately adiabatic wall temperature conditions. Values of the stagnation and freestream properties, and boundary layer parameters measured approximately 1δ upstream of the compression corner are listed in Table 1

Parameter		
M_∞	4.92	4.92
P_o	340 psia.	2.34 MPa
T_o	640° R	356 K
U_∞	2530 ft/s	770 m/s
δ	0.76 in.	1.93 cm
Re_δ	1.29×10^6	1.29×10^6
δ^*	0.36 in.	0.90 cm
θ	0.030 in.	0.075 cm
$C_f \times 10^3$	0.76	0.76
Π	0.44	0.44

Table 1: Freestream Flow Conditions and Turbulent Boundary Layer Properties

below.

Models

The SWTBLI was generated by a 28° unswept compression corner. This particular interaction was selected because it produces a nominally two-dimensional flowfield that has been studied in detail in this facility. The model is 6.25δ wide and 1.97δ high and it can be adjusted streamwise relative to a fixed spanwise row of transducers upstream. This model, with the Wheeler doublets upstream, is shown in figure 1. Fences, approximately 0.16δ thick, were attached to the model to prevent spillage and to isolate it from the tunnel side-wall boundary layers. The leading edges of the fences were beveled to prevent shocks from interfering with the interaction. The fences extended 3.95δ upstream of, and 1.32δ above the compression corner model.

An array of four Wheeler doublets was placed 15.8δ (X_{vg} = -15.8) upstream of the compression corner as shown in figure 1. In a preliminary set of experiments, VG positions in the range -21 ≤ X_{vg} ≤ -11 were examined. No significant variations in the intermittent region flowfield were observed as the variations of σ_{pw} and f_c were less than 5% when comparing equivalent locations in the intermittent region. Therefore, it was concluded that within the range -21 ≤ X_{vg} ≤ -11, the position of the VGs has only a second order effect on the separation shock dynamics. Each doublet is made of two Wheeler singlets placed inline. McCormick's results indicated that the doublet arrangement is more effective than the singlet in perturbing the mean interaction scale; therefore, the doublet arrangement was used exclusively in these tests. Each singlet is 0.33δ high, 2.37δ long, and 1.64δ wide. This ratio of length to width to height was selected to match that used by McCormick because at the time these experiments were begun, the computational results of Barber, et al. were not available. When placed inline, the singlets were overlapped by 0.26δ (see fig. 1) giving a total doublet length of 4.47δ.

The VGs were attached to the tunnel floor using Devcon Instant Adhesives Super Glue. To insure that the spanwise placement of the VGs was repeatable, a template was used to place them symmetrically about the tunnel centerline. During tests in which wall pressure data were taken on the tunnel floor, it was necessary to move the compression corner model to make measurements at various locations in the intermittent region. As a result, there is a ± 1.7% variation in X_{vg}. Since X_{vg} had been
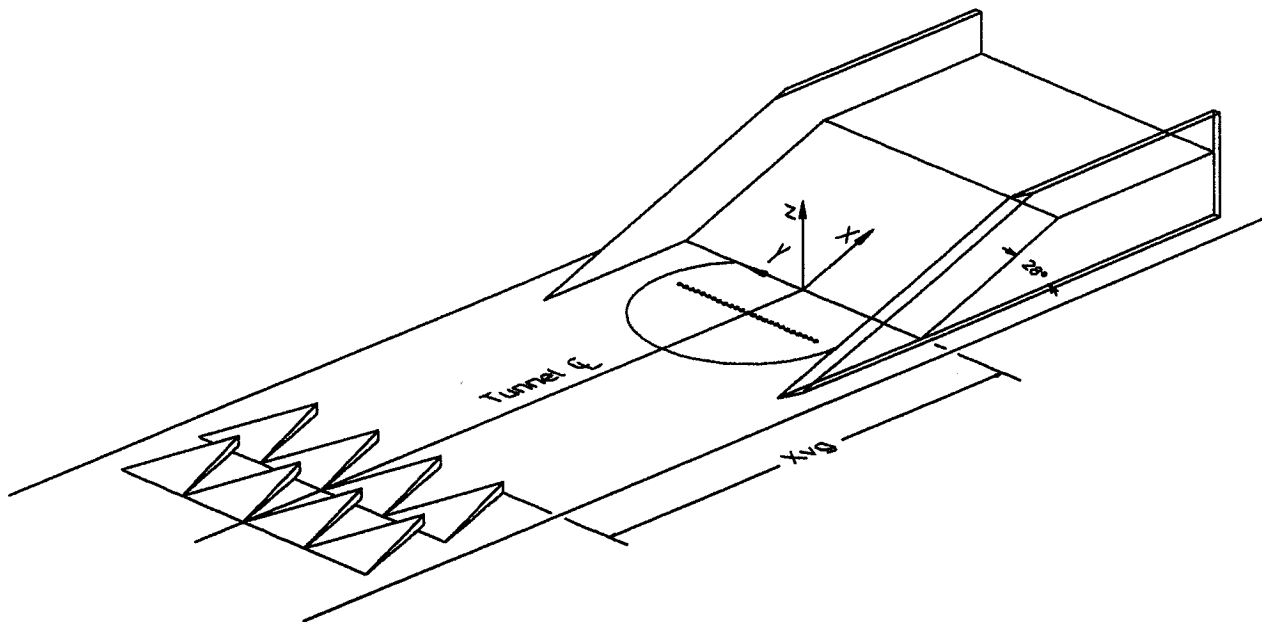

Figure 1: 28 Degree Unswept Compression Corner Model with VGs Upstream

4

shown to have only second order effects on the shock dynamics, the effects of the shift in X_{vg} are judged negligible.

<u>Instrumentation and Data Acquisition</u>

Wall pressure measurements were made using Kulite model XCQ-062-15A (0-15 psia.) and XCQ-062-50A (0-50 psia.) transducers. The outside diameter of these transducers is nominally 0.0625 in. (0.16 cm). The pressure sensing element is a 0.028 in. (0.071 cm) diameter silicon diaphragm with a Wheatstone bridge atomically diffused into it. With their protective screens in place, these transducers have a frequency response of about 50 kHz when mounted flush with the tunnel wall. They were installed in a 3.375 in. (8.57 cm) diameter circular instrumentation plug that could be inserted flush with the tunnel floor (see figure 1). When transducer ports were not being used, they were filled with dummy plugs. To insure that the transducers and dummy plugs were flush with the instrumentation plug face, the installation was inspected using a magnifying glass.

The instrumentation plug could be rotated such that the transducers were either in a streamwise or spanwise row. Because the undisturbed (or baseline) interaction is nominally 2-D,[19] it was investigated using transducers placed in a streamwise row. However, the addition of the VGs upstream introduces significant three-dimensionality into the incoming boundary layer. Therefore, when investigating the disturbed interaction, the transducers were placed in a spanwise row so that the effects of this 3-D boundary layer could be ascertained.

The output of the transducers was amplified and low-pass filtered at a cut-off frequency of 50 kHz. to prevent aliasing. The transducers were statically calibrated daily. During the calibration procedure the amplifier bias and gain were set so that the amplified output would span the entire 0-4.096 V. range of the A/D converter. The maximum amplitude of the electronic noise at the input to the A/D converter was less than 10 mV corresponding to a typical signal to noise ratio of about 200. The LeCroy 6810 Waveform Recorder employs a 12-bit A/D converter and was operated at a sampling frequency of 200 kHz/channel. During a typical run, eight channels of data were sampled simultaneously with 512 records (1024 points/record) of data acquired per channel.

Mean pitot probe traverses were also made of the incoming boundary layer using a pitot rake with seven tubes in a spanwise row. Individual tips were spaced 0.5 inches (1.27 cm) apart. The rake can be shifted ±0.25 in. (0.64 cm) spanwise such that the boundary layer can be studied up to ±1.75 inches (4.45 cm) off centerline. Due to geometric limitations, measurements could not be made below Z=0.013. The pitot pressure measurements were made using Kulite CTQH-187-50A transducers which have a range of 0-50 psia and are located inside the rake approximately 2.5 in. (6.35 cm) downstream of the pitot tube tips. The calibration procedure was the same as that used for the wall pressure transducers. The vertical displacement of the pitot rake was measured using a calibrated Linear Variable Differential Transformer (LVDT). Data were simultaneously sampled at 200 Hz/channel and a traverse of the boundary layer took approximately ten seconds. During the traverse, the freestream stagnation pressure variation was typically less than ±0.6%.

Data Analysis

Besides computing the basic statistical properties of the data (mean, standard deviation, etc.), the data taken in the intermittent region were also analyzed to determine the dynamics of the separation shock foot. The algorithm for quantifying the shock dynamics is thoroughly discussed in reference 20 and will only be summarized below.

A typical wall pressure signal measured in the intermittent region is shown in figure 2. The low pressure segments of the signal correspond to times during which the transducer is exposed to the undisturbed boundary layer pressure. Higher pressures are recorded when the separation shock is upstream of the transducer. The algorithm first determines the mean and RMS ($\bar{P}_{w,0}$ and $\sigma_{pw,0}$, respectively) of the undisturbed boundary layer portion of the intermittent wall pressure signal. Two thresholds are then defined: $T_1 = \bar{P}_{w,0} + 3\sigma_{pw,0}$ and $T_2 = \bar{P}_{w,0} + 6\sigma_{pw,0}$. These thresholds have been selected so that the counting of turbulent fluctuations as shock crossings is largely avoided. The entire wall pressure signal is analyzed using these thresholds. When the pressure rises above T_2, the separation shock has moved upstream of the transducer and a rise time, t_r, is recorded. When the

5

pressure falls below T_1, the separation shock has moved downstream of the transducer and a temporary fall time is recorded. The algorithm then steps back in time to determine when the T_2 threshold was crossed. This time is then recorded as the actual fall time. T_1 is used to determine the temporary fall time so that turbulent fluctuations in the separated flow downstream of the shock are not counted as shock crossings. The algorithm steps back in time so that a common threshold is used to compute the rise and fall times.
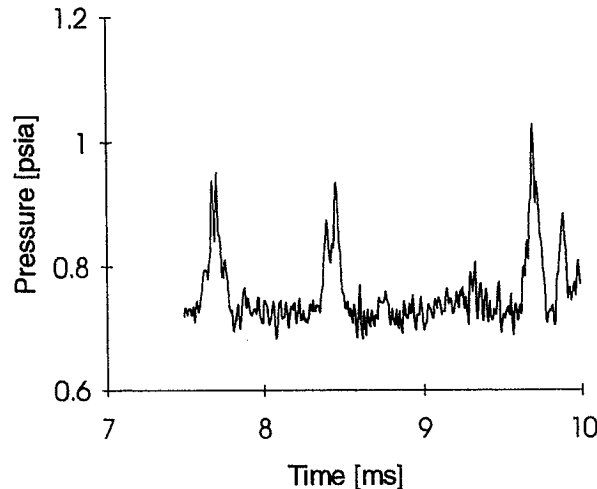
Figure 2: Typical Wall Pressure Signal Measured in the Intermittent Region

Based on the rise and fall times several parameters can be defined to describe the shock dynamics. The intermittency, γ, is defined as the fraction of time the separation shock is upstream of the transducer and is computed using equation 1.

$$\gamma = \frac{1}{t_{total}} \sum_{i=1}^{N} (t_f - t_r)_i \tag{1}$$

An average period between shock crossings as the shock moves upstream can also be defined using equation 2.

$$T_{ave} = \frac{1}{N} \sum_{i=1}^{N-1} (t_{r,i+1} - t_{r,i}) \tag{2}$$

Finally the zero crossing frequency, f_c, is the inverse of the average period. It is a measure of how frequently, on average, the separation shock crosses a given point in a given direction and it gives an initial indication of the frequency content of the intermittent signal. For instance, a higher zero crossing frequency usually indicates that the dominant frequency band of the signal has shifted to higher frequencies.

In this study, the upstream boundary of the intermittent region (i.e., the upstream influence line) is defined as the location where the intermittency is 1%. Similarly, the downstream boundary, which in practice is very close to the separation line, is defined as the location where the intermittency is 99%. The distance between these boundaries is the intermittent region length.

Erengil and Dolling[21] have shown that the error function is a good fit to the intermittency data. Using a code written by Gonsalez[22] the intermittency data were least-squares curve fit such that the upstream and downstream boundaries of the intermittent region and its length could be systematically determined. A second code written by Gonsalez was used to apply a Fourier series curve fit to the zero crossing frequency data so that $f_{c,max}$ could also be estimated consistently.

To evaluate the VGs' effectiveness in shifting the energy of the wall pressure fluctuations to a higher frequency band it is necessary to quantify the fraction of the variance in a given frequency band. The spectral density function, G(f), describes how the mean squared value of the wall pressure is distributed

in the frequency domain. The integral of G(f) over a prescribed frequency band divided by the overall variance of the wall pressure gives the fraction of energy, β, due to wall pressure fluctuations in the frequency band. According to Pozefsky, et al., the typical resonant frequency band for aircraft skin panels is 100-500 Hz. The above technique is used to determine the effectiveness of the VGs in decreasing β in this frequency band.

Results

Undisturbed Interaction

The separation shock motion in SWTBLIs has been characterized by Erengil and Dolling as having two components.[23] The first is a low-amplitude, high frequency jitter motion produced by fluctuations in the instantaneous pressure ratio across the separation shock. This jitter is superimposed upon a large-scale, low-frequency motion produced by pulsation of the separated flow. The combination of these two types of motion produces the observed streamwise variation in flow properties.

The mean wall pressure distribution through the intermittent region is shown in figure 3 and the wall pressure RMS, the intermittency, and the zero crossing frequency distributions are shown in figure 4. The intermittent region is 1.41δ long with upstream influence 2.94δ upstream of the compression corner leading edge. The maximum RMS of the wall pressure, nondimensionalized by P_∞, and the maximum zero crossing frequency are 0.48 and 0.86 kHz, respectively.
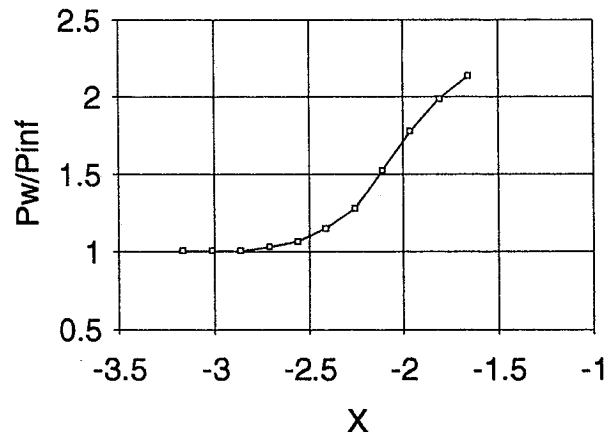

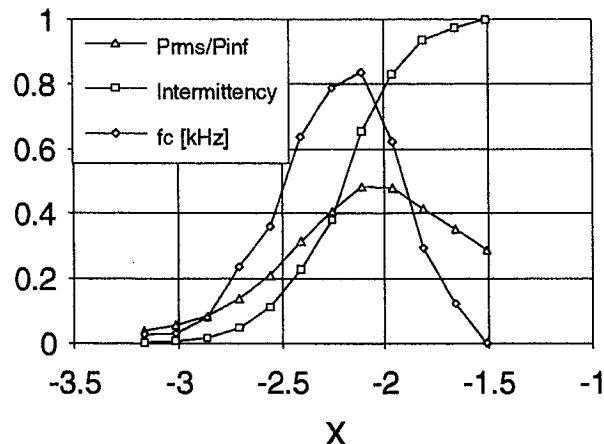Figure 3: Mean Wall Pressure Distribution in the Undisturbed Interaction

Figure 4: Wall Pressure RMS, Zero Crossing Frequency, and Intermittency Distributions in the Undisturbed Interaction

7

The fraction of the overall variance contained in the 100-500 Hz. frequency band at all stations in the intermittent region is shown in figure 5. This band, as noted earlier, is the frequency band of interest. Over the range of $0.1 \leq \gamma \leq 0.85$ about 35% of the total wall pressure fluctuation energy is contained in this band.
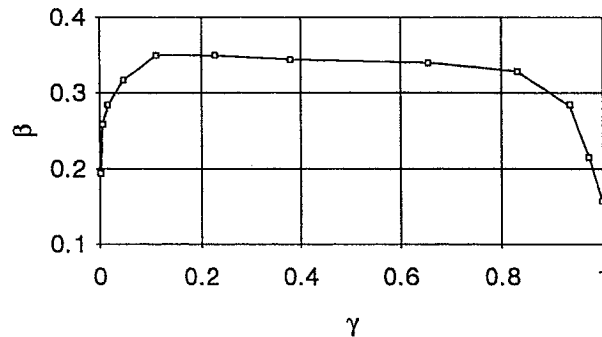

Figure 5: Fraction of Energy in the 100-500 Hz Frequency Band

To understand the shape of the distribution in figure 5, it is necessary to review the wall pressure power spectra through the intermittent region as shown in figure 6. Within the intermittent region, a transducer is exposed to three flow regimes that effect the power spectrum. When the separation shock is downstream of the transducer, it is exposed to low-amplitude, high-frequency fluctuations in the
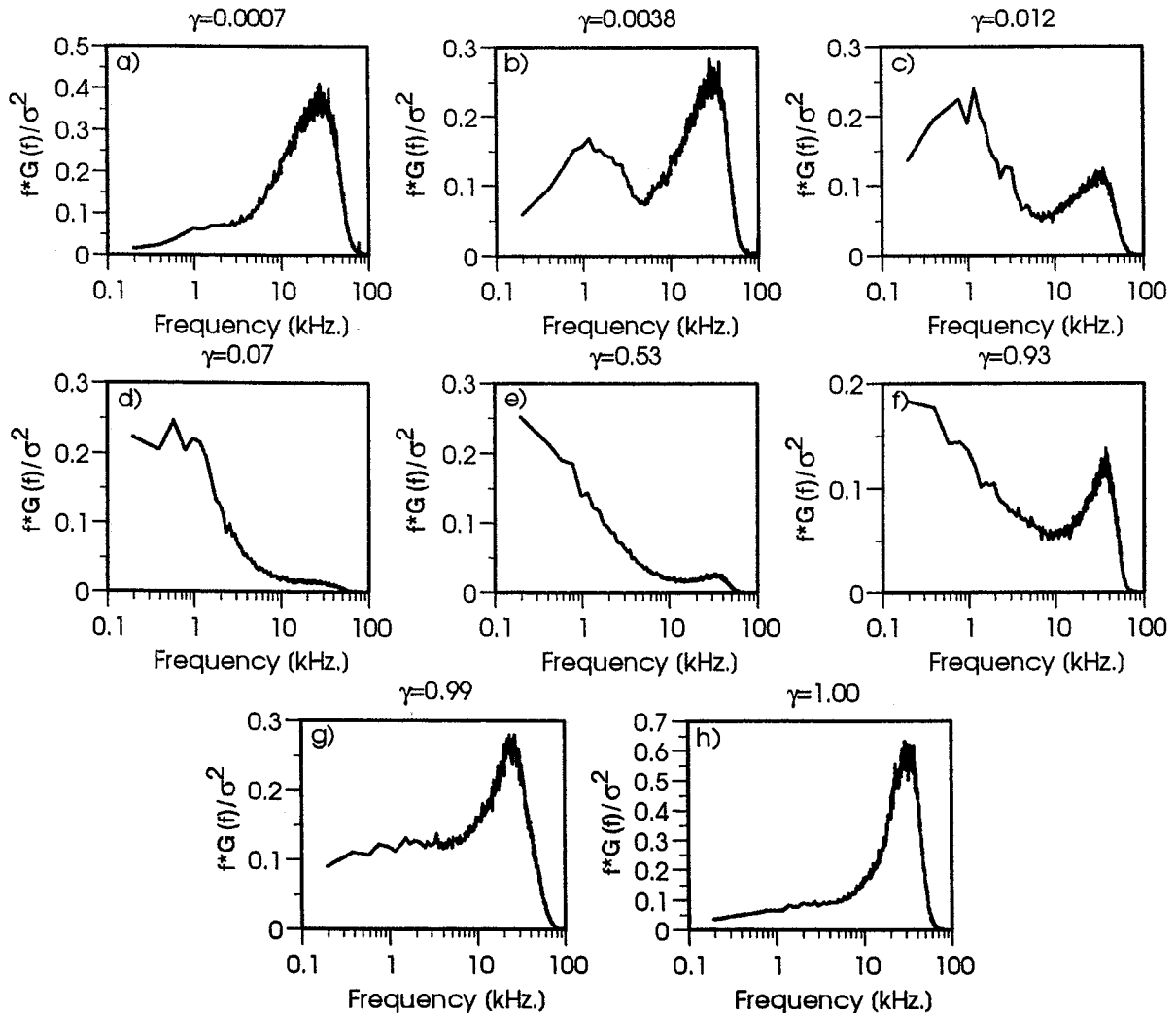
Figure 6: Wall Pressure Power Spectra in the Intermittent Region

8

incoming boundary layer. When the separation shock is upstream of the transducer, it is exposed to higher-amplitude, high-frequency fluctuations due to amplified turbulence in the separated shear layer. Finally, it is exposed to high-amplitude, low-frequency fluctuations due to the motion of the separation shock over it. The relative weighting of these three components at different stations controls the shape of the power spectra in the intermittent region.

At very low intermittencies, there is little energy in the 100-500 Hz band because almost all the energy is due to turbulent fluctuations in the incoming boundary layer at frequencies greater then 10 kHz (fig. 6a). Consequently, the fraction of energy in the 100-500 Hz band is low. As intermittency increases, the role of the separation shock becomes increasingly important as does the role of the amplified turbulence downstream of the separation shock. At low intermittencies (figs. 6b,c) the contributions from the separation shock motion and the incoming boundary layer are evident.

As intermittency increases further, the fluctuations due to separation shock motion add significant energy to the wall pressure signal (as evidenced by increased RMS levels) and dominate it. This added energy is at low frequencies causing a shift in the normalized power spectrum to lower frequencies as seen in figures 6d,e. This added energy causes the rapid increase in the fraction of energy in the 100-500 Hz band between $\gamma=0$ and 0.1.

The dominance of pressure fluctuations due to separation shock motion produces the broad-band peak in the fraction of energy in the 100-500 Hz band over the range $0.1 \leq \gamma \leq 0.85$. Near the downstream edge of the intermittent region, fluctuations in the separated shear layer become more significant and fluctuations due to the separation shock motion become less significant (figs 6f-h). The net result is a decrease in the total energy and a decrease in the fraction of energy in the 100-500 Hz band.

Marshall and Dolling[19] studied the spanwise variation of intermittent region properties. Data from their study were analyzed with the same codes used to analyze the data obtained for the present study. Marshall and Dolling's experiments were conducted in the same facility under essentially the same freestream conditions further upstream with a thinner boundary layer.

Figures 7 and 8 show the spanwise variation of intermittency and normalized wall pressure RMS obtained using Marshall and Dolling's data. It can be seen that the interaction is nominally two dimensional with significant departures from two-dimensionality caused by three-dimensionality in the incoming boundary layer occurring only at the edges. There is no spanwise periodicity which is an important distinction between these results and those to be presented later.
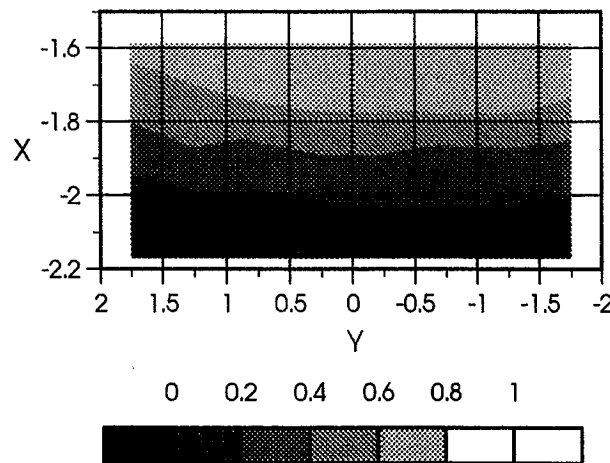

Figure 7: Spanwise Variation of Intermittency in the Undisturbed Interaction
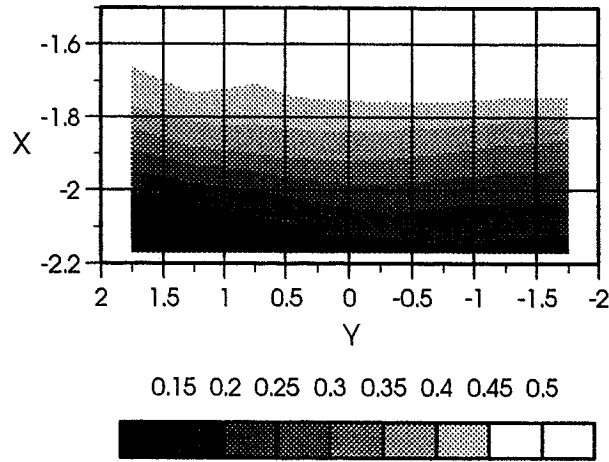
Figure 8: Spanwise Variation of Wall Pressure RMS in the Undisturbed Interaction
(normalized by P_∞)

Effect of the VGs on the Incoming Boundary Layer

Mean pitot pressure surveys of the boundary layer were made with and without the VGs upstream. Figure 9 shows that the undisturbed boundary layer pitot pressure distribution is essentially uniform spanwise; there is no indication of spanwise periodicity. The velocity profiles derived from these pitot surveys are good fits to Law of the Wall/Law of the Wake at all spanwise stations.
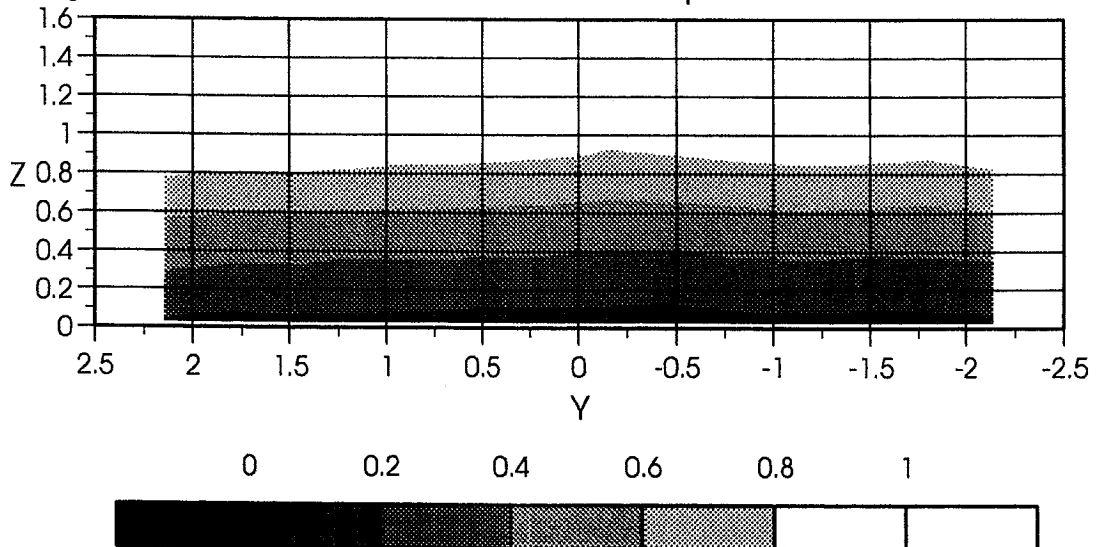
Figure 9: Undisturbed Incoming Boundary Layer Pitot Pressure (normalized by $P_{t,\infty}$)

Pitot pressure measurements were made at two stations downstream of the VGs to obtain an indication of the streamwise development of the disturbed boundary layer. These surveys show that the VGs fill out the incoming boundary layer in certain regions and produce momentum deficient regions downstream of the VG apexes. Figure 10 shows the disturbed normalized boundary layer pitot pressure distribution 6.6δ downstream of the VGs. There is a distinct three-dimensional pattern in the disturbed boundary layer. Downstream of the VG apexes at Y=±0.82, there is a dominant low-momentum region which, although not evident in the contour plots, causes a substantial thickening of the boundary layer. These low-momentum regions are interspersed with regions of high momentum fluid. The pitot pressures in this region are higher (maximum increase: 28%) than those measured at the same location in the undisturbed boundary layer. The near-wall region (Z<0.15) is largely unaffected by the vortex generators.

10

There is little spanwise variation in measured pitot pressure near the wall and the magnitudes are the same for the undisturbed and disturbed boundary layers.
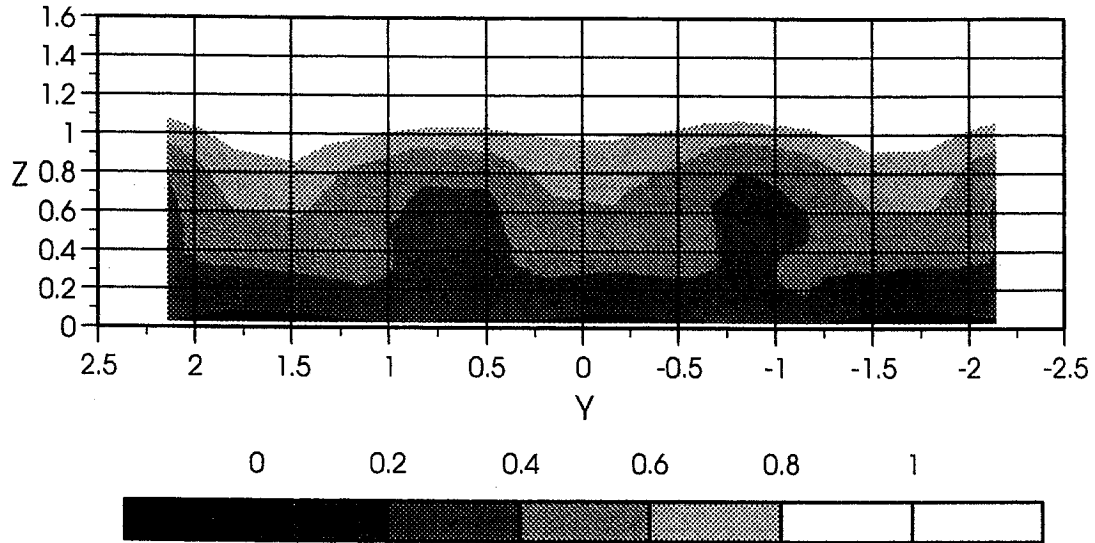

Figure 10: VG disturbed Boundary Layer Pitot Pressure Surveys Measured 6.6δ Downstream of the VGs (normalized by $P_{t,\infty}$)
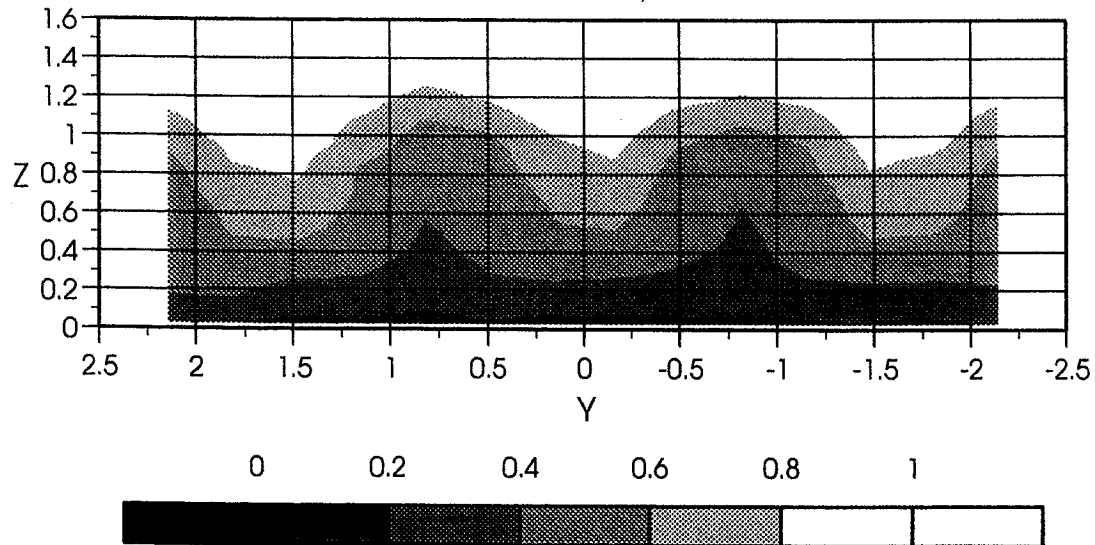

Figure 11: VG disturbed Boundary Layer Pitot Pressure Surveys Measured 14.5δ Downstream of the VGs (normalized by $P_{t,\infty}$)

Pitot pressures measured 14.5δ downstream of the VGs, shown in figure 11, are similar to those seen in figure 10. The most noticeable difference seen in figure 11 is that there is a substantial spanwise thinning of the low-momentum regions downstream of the VG apexes. The maximum increase in pitot pressure due to the action of the vortices at this streamwise station is 39% indicating that the vortices are still coherent and acting to fill out the boundary layer between 6.6δ and 14.5δ downstream.

The thinning of the low-momentum region downstream of the apexes indicates that there is substantial crossflow within the boundary layer. Computational and experimental results presented by Barber, et al.[16] indicate that transverse velocities could be as high as $0.2U_\infty$ at 10 VG heights downstream of the vortex generators. In addition, there could be pressure gradients within the boundary layer associated with this crossflow. Therefore, with the present data, it is not appropriate to derive a

11

velocity field from the pitot pressures because no simultaneous static pressure or transverse velocity measurements were made. It is assumed that higher pitot pressure is indicative of a higher streamwise velocity component everywhere within the boundary layer, but this cannot be proven without a more thorough set of measurements.

It was previously mentioned that in preliminary experiments the location of the VGs was found to have only a second order effect on the separation shock dynamics. The striking similarity between figures 10 and 11 indicates why. As the boundary layer travels from 6.6δ to 14.5δ downstream of the VGs it's structure does not change substantially. The vortices continue to energize the boundary layer at 14.5δ downstream and do not appear to be moving away from the wall rapidly. Consequently, these VGs have the potential to be effective over a wide range of streamwise locations.

Effect of the VGs on the Intermittent Region Size and Shape

The placement of Wheeler doublet vortex generators upstream of the SWTBLI has a major effect on the size and shape of the flowfield upstream of the corner. Before viewing contour plots of properties in the intermittent region it is useful to note that the VG apexes were located at Y=±0.82 and ±2.47. Also recall that the array of VGs was symmetric about the wind tunnel centerline (Y=0).

The most obvious effect is that the interaction is no longer two-dimensional. Consequently, there is significant variation in the spanwise properties of the intermittent region. Before looking at these spanwise variations in detail, it is possible to make a few general observations about the changes and their relationship to the undisturbed interaction. In the presence of the VGs, the maximum length of the intermittent region is 0.55δ and the maximum upstream influence is 1.16δ. Compared to the undisturbed interaction, these lengths are 60% shorter. The minimum intermittent region length and upstream influence are 0.45δ and 1.10δ, respectively, which are 67% and 62% shorter than in the undisturbed interaction.

Figures 12 and 13 show the mean pressure and intermittency distributions through the interaction. The overall pressure rise through the intermittent region is less than in the undisturbed interaction and occurs over a significantly shorter distance. At S, $\bar{P}_w/P_\infty$ is approximately 0.15-0.25 less which indicates that the separation shock is weaker when the VGs are upstream. The most obvious change in the interaction is that the VGs have made the interaction spanwise periodic. This periodicity correlates with the locations of certain geometric features of the VGs upstream. The initial rise in pressure and intermittency first occurs in the regions of the interaction downstream of the VG apexes. This indicates that the VGs are least effective in the region downstream of their apexes. This is to be expected as the counter-rotating vortices deposit low momentum fluid in this region.
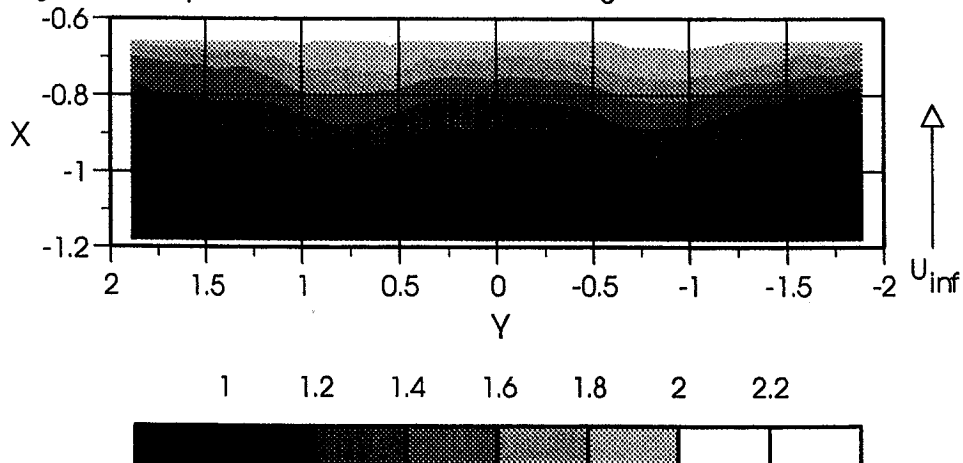

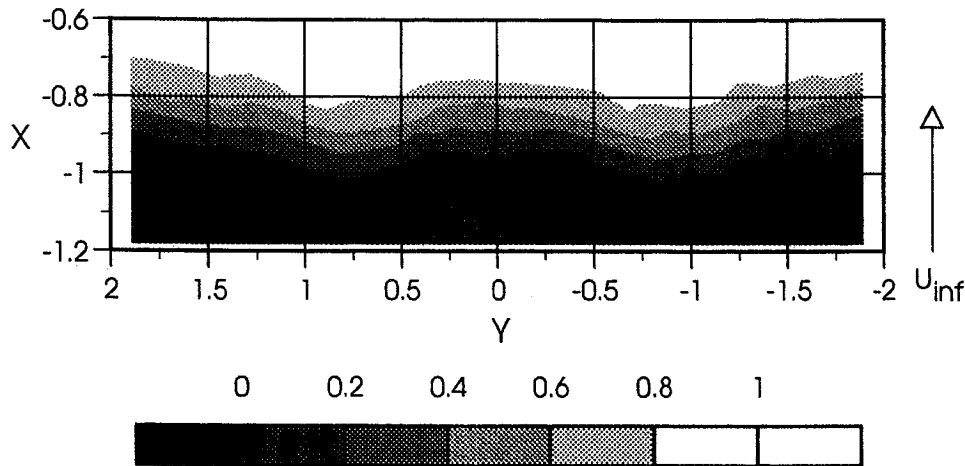Figure 12: Mean Wall Pressure Distribution in the Intermittent Region (normalized by P_∞)

Figure 13: Intermittency Distribution

The effect of the VGs increases away from the apexes. In the region between the apexes (-0.82 ≤ Y ≤ 0.82) the initial rise in pressure and intermittency moves downstream. To within experimental error, there is no spanwise variation in mean pressure for -0.38 ≤ Y ≤ 0.38. Outside the apexes at Y=±0.82, the intermittent region moves further downstream due to nonuniformities in the incoming boundary layer.

The downstream shift of the intermittent region outside the VG apexes is consistent with the shift observed in the undisturbed interaction. It was previously shown in figures 7 and 8 that as the distance from the tunnel centerline (Y=0) increases, the interaction becomes increasing three-dimensional. Figure 7 shows that the departure from two-dimensionality is greatest on the left side (Y>0) of the tunnel. Similarly, figure 13 shows that the left side of the tunnel has a greater downstream shift than the right side of the tunnel.

In the following discussion, the regions outside the first set of apexes (Y= ±0.82) will be shown in the figures to demonstrate the spanwise periodic structure of the interaction. However, to avoid effects due to three-dimensionality in the undisturbed tunnel floor boundary layer, only the region between the apexes will be considered when evaluating the effectiveness of the VGs in reducing fluctuating pressure loads.

Spanwise variation of the intermittent region length and upstream influence and separation lines were computed from the intermittency data. Initially, these quantities were computed using the error function curve fit to the raw intermittency data. The results of this analysis were inconclusive as scatter in the data was of the same order as the relatively small spanwise variation in these quantities. To reduce the effects of the scatter, two averaging techniques were employed.

The first technique was to compute the different lengths (L_i, UI, and S) at each spanwise location from the error function fit to the raw intermittency data. These lengths were averaged with the lengths computed at adjacent stations (i.e., the stations to the left and right) to produce corrected lengths for the station of interest. The second technique was to first average the raw intermittency data with data at adjacent stations and then apply the error function fit to obtain the desired lengths. Averaging the intermittency data (figure 14) reduces scatter by smoothing the curves without suppressing maxima or minima in the data. The spanwise variation of intermittent region length, upstream influence and separation lines obtained using the different averaging techniques were nearly identical. The average absolute difference between lengths computed using the two techniques were 1.7%, 0.34%, and 0.75% for L_i, UI, and S, respectively.

The spanwise variations of the intermittent region length, upstream influence, and separation line are shown in figure 15. The spanwise variations of these lengths are spatially periodic which is consistent with the previously observed results. The minimum and maximum intermittent region lengths are approximately 0.45δ and 0.49δ (when only considering the region between VG apexes). This spanwise variation of L_i is remarkably small when one considers the magnitude of the variations in the incoming boundary layer. The minima occur downstream of the VG apexes while the maximum is located along the line of symmetry between the VGs.
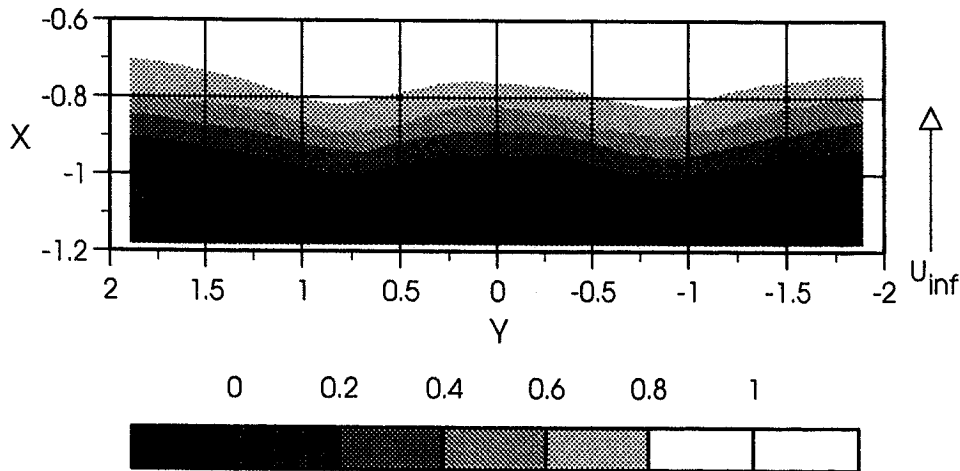
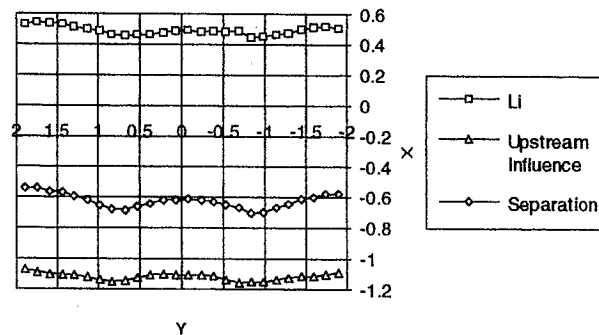Figure 14: Averaged Intermittency Data Distribution

Figure 15: Spanwise Variation of Intermittent Region Length, Upstream Influence, and Separation

The observed variations in L_i are driven by variations in both the upstream influence and separation lines. To clarify the following discussion, it is worth pointing out that the instantaneous separation point is almost immediately downstream of the separation shock foot, not at S.[24] S is called the separation line because it appears as a well defined line in surface flow visualization techniques. Unsteady measurements show that this well defined line occurs very close to where $\gamma=1$, so that using the latter location as an indication of S is appropriate.

The upstream influence line is nearly straight with small shifts upstream in the regions downstream of the VG apexes. Like UI, S shifts upstream in the region downstream of the VG apexes. However, the shift in S is greater than that of UI and as a result, the intermittent region becomes smaller downstream of the VG apexes. The upstream shift of S downstream of the VG apexes is consistent with the behavior of the boundary layer downstream of the VGs. The lowest momentum fluid in the incoming boundary layer is downstream of the apexes. Thus, the separated region length should be greater downstream of the apexes. However, it is not clear at this stage why the upstream influence line does not shift forward an equal or greater amount than the separation line.

Effect of the VGs on Fluctuating Pressure Loads

The vortex generators have two effects on the fluctuating pressure loads produced by the SWTBLI. First, the magnitude of the maximum wall pressure RMS has been reduced. Second, the frequency range of the fluctuating loads in the disturbed interaction has been shifted to a higher band. In the undisturbed interaction, the upper bound of the dominant frequency band is about 1 kHz but this bound shifts to about 5 kHz in the disturbed interaction. Due to a frequency resolution of 48.8 Hz, it is not possible to quantify the shift in the lower bound of the dominant frequency band. However, visual inspection of the spectra indicate that this lower bound has also shifted to a higher frequency.
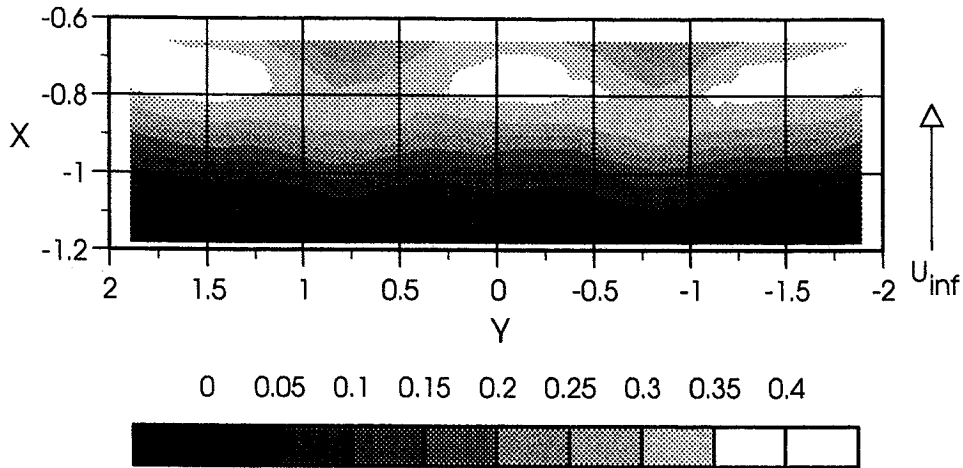
14

Figure 16: Wall Pressure RMS Distribution in the Intermittent Region (normalized by P_∞)
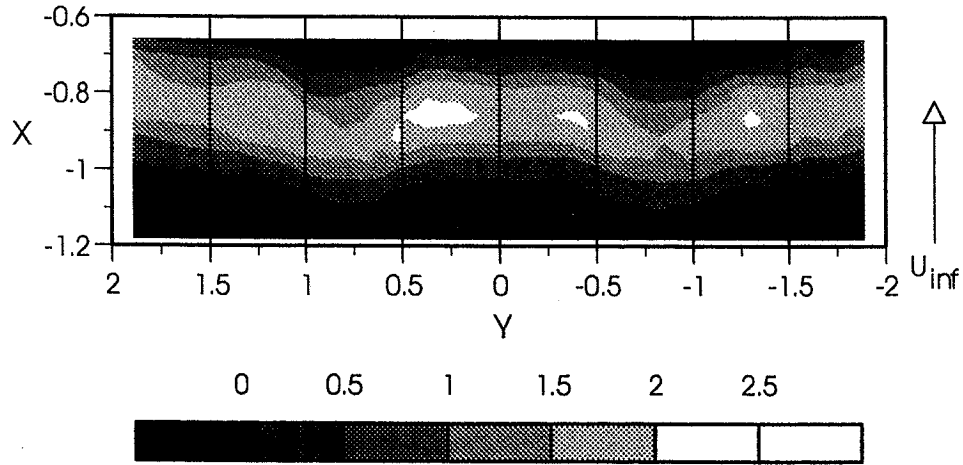

Figure 17: Zero Crossing Frequency [kHz] Distribution in the Intermittent Region

Figure 16 shows the wall pressure RMS in the intermittent region. Like the mean wall pressure and intermittency distributions, the wall pressure RMS distribution is spatially periodic and this periodicity is consistent with the locations of the vortex generators upstream. RMS levels first rise above the turbulent boundary layer level downstream of the VG apexes. The highest RMS levels occur between the VG apexes near the downstream edge of the interaction. The maximum σ_{pw}/P_∞ is 0.37 which is a decrease of 23% compared to the undisturbed interaction. The peak RMS downstream of the apexes is slightly lower at 29% below the undisturbed interaction peak RMS. This reduced σ_{pw}/P_∞ is due to a smaller separated flow having a weaker separation shock.
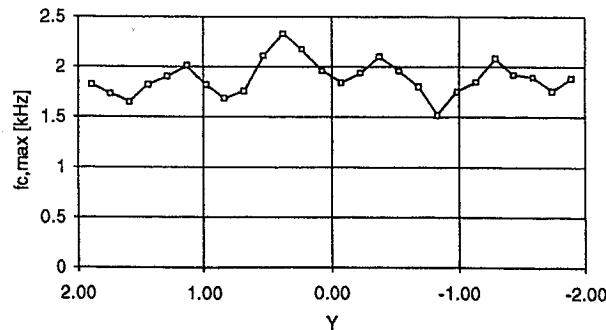

Figure 18: Spanwise Variation of the Maximum Zero Crossing Frequency

15

The zero crossing frequency distribution in the intermittent region is shown in figure 17 and it too is periodic. As previously mentioned, the zero crossing frequency is a measure of how often, on average, the separation shock crosses a given point in a given direction and more importantly indicates shifts in the dominant frequency band of the wall pressure fluctuations. The overall maximum zero crossing frequency is 2.33 kHz which is a 171% increase over $f_{c,max}$ in the undisturbed interaction. As with undisturbed interaction, the maximum zero crossing frequency occurs near 50% intermittency.

Maximum zero crossing frequencies across the interaction span are shown in figure 18 and were obtained by curve fitting the raw zero crossing frequency data. While there is some scatter in the data, a pattern, consistent with the other results, is apparent. Local maxima in $f_{c,max}$ occur approximately halfway between the VG apex and tunnel centerline while local minima occur downstream of the VG apex.

The shift to higher zero crossing frequencies is due to enhanced jitter-type motion of the separation shock. Shown in figure 19 (Baseline PDF was obtained from data taken by Erengil and published in reference 25.) are probability density functions of the separation shock period at various spanwise locations at 50% intermittency. These PDFs are representative of those computed at other locations in the intermittent region. As f_c increases, the PDFs indicate that the separation shock motion has more shorter periods (i.e. higher frequency, jitter-type motion). It is this increase in the high frequency jitter motion which is responsible for the increase in the zero crossing frequency. Recall that separation shock jitter is caused by fluctuations in the instantaneous pressure ratio across the separation shock. Thus, the VGs, in addition to energizing the mean boundary layer, must also enhance turbulent fluctuations in the incoming boundary layer needed to cause fluctuations in the instantaneous pressure ratio across the separation shock.

Increased jitter motion is not uniform across the VG span. It can be seen in figure 19 that there are three PDFs at f_c=1.8 kHz. The two PDFs at approximately symmetric locations about the VG apex (Y=-0.68 and -0.98) overlay each other. However, the PDF near the tunnel centerline (Y=-0.076) has a significantly higher peak at the shortest periods indicating that the separation shock has more jitter at this station than at Y=-0.86 and -0.98. However, in order for all three of these stations to have the same zero crossing frequency (i.e., the same average period), the separation shock at Y=-0.076 must also have more low frequency motions. This would suggest that there are also spanwise variations in the low
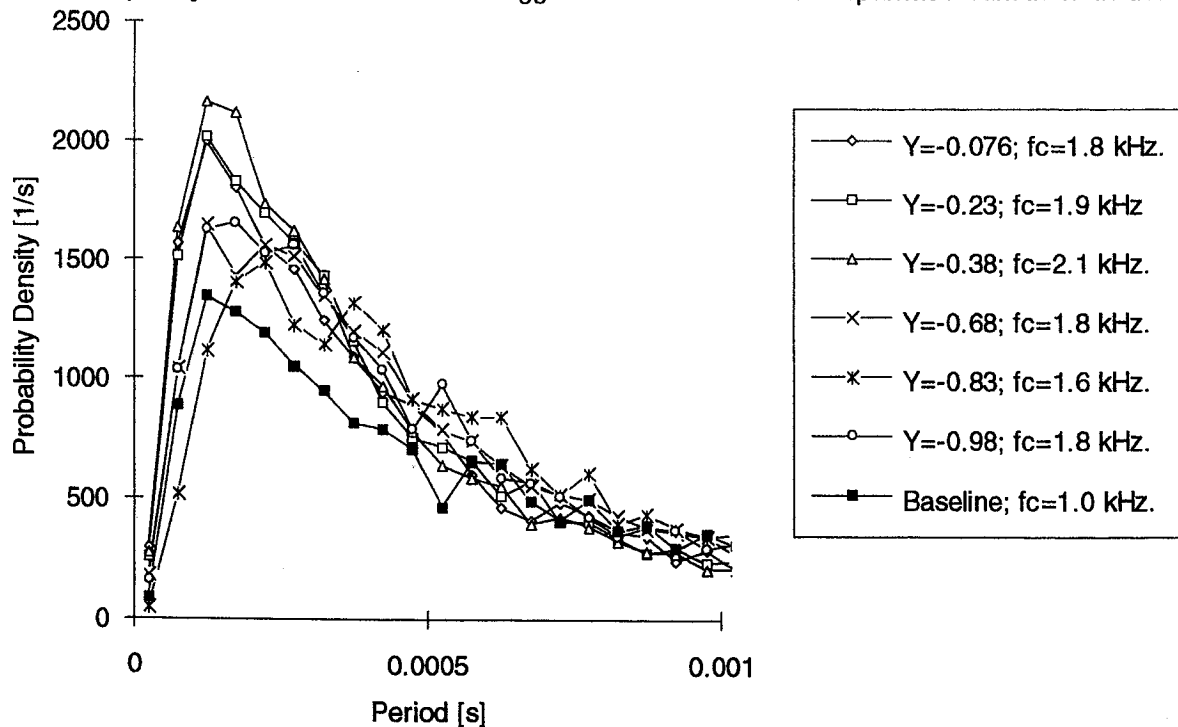

Figure 19: Spanwise Probability Density Functions of the Separation Shock Period

frequency separation shock motion which is caused by expansion and contraction of the separation bubble.

Gonsalez and Dolling[17] found that the intermittent region length and maximum zero crossing frequency are inversely proportional and that their relationship could be expressed in terms of a characteristic Strouhal number given by $L_i(f_{c,max})/U_\infty$. For the boundary layer used in their study, which is essentially the same as the undisturbed boundary layer in the present study, this Strouhal number is 0.0225 with a standard deviation of 0.00306. This relationship between $f_{c,max}$ and L_i results from shock velocities being essentially the same in a number of different types of SWTBLIs with the same incoming boundary layer, irrespective of the intermittent region size.

Figure 20 compares the Strouhal numbers for the present study with those presented by Gonsalez and Dolling. To be consistent with Gonsalez and Dolling, for this figure L_i is defined as the distance from 5% to 95% intermittency. The average Strouhal number for the present study is 0.0164 which is 2σ below that obtained by Gonsalez and Dolling. Since the freestream velocities for these two studies are the same, the difference must lie in the product of $f_{c,max}$ and L_i being less for the present study. This means that for a given L_i, $f_{c,max}$ is less, on average, than that observed by Gonsalez and Dolling. This suggests that the shock velocities are lower in the disturbed interaction.
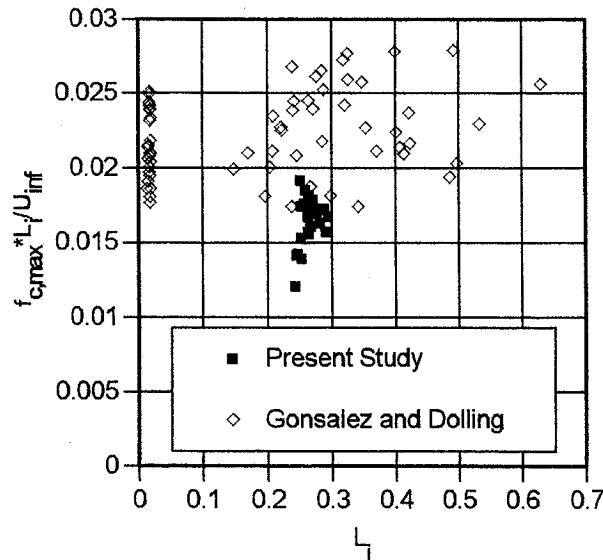
Figure 20: Relationship Between L_i and $f_{c,max}$ in Terms of Strouhal number

The enhanced separation shock jitter is responsible for shifting the dominant frequency band of the wall pressure fluctuations to a higher band. This shift results in reduced wall pressure fluctuation energy in the 100-500 Hz range. Figure 21 shows the distribution of the fraction of energy due to wall pressure fluctuations in the 100-500 Hz band, the typical skin panel resonant frequency band. Like the undisturbed interaction, this distribution has a broad band peak but at a lower level. β_{max}, which occurs downstream of the VG apexes and along the tunnel centerline, is 0.31, an 11% decrease as compared to the undisturbed interaction. Between the centerline and VG apexes, the maximum β along a streamwise cut through the intermittent region was observed to decrease to a minimum of 0.27 (23% less than undisturbed value).

The highest zero crossing frequencies have been found in the region between the centerline and the VG apexes. It is in this region that the separation shock jitter motion has been enhanced the most. Thus, the decrease in β between the centerline and apexes is consistent with the previously discussed enhanced jitter motion of the separation shock.
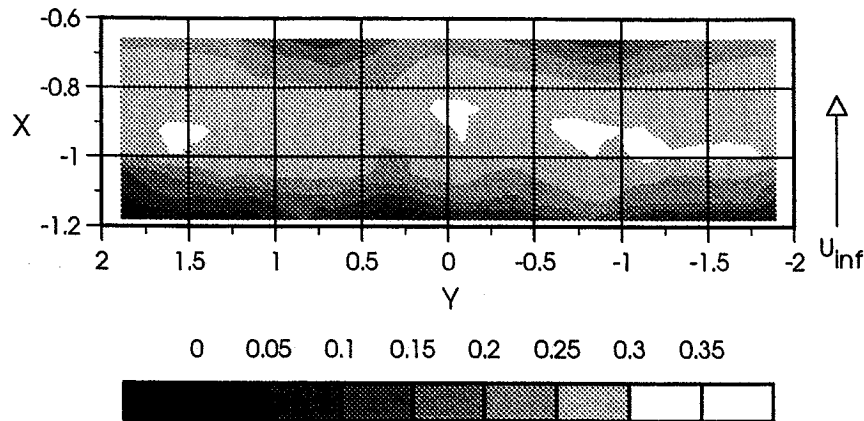
17

Figure 21: Fraction of Wall Pressure Fluctuation Energy in the 100-500 Hz. Band in the Intermittent Region

Conclusions

Wheeler Doublets add three-dimensionality to an otherwise two dimensional shock wave turbulent boundary layer interaction. The VGs are effective in reducing and changing the frequency content of separation shock induced fluctuating pressure loads produced by compression corner induced turbulent separation. The magnitude of the maximum loading was reduced by 23-29% and the amount of energy in the low frequency band (100-500 Hz.) was reduced by 11-23%. Additionally, the area exposed to high loads is reduced by 60% due to the downstream shift of the upstream influence line.

Pitot pressure surveys suggest that regions of the incoming boundary layer have a fuller profile. This fuller profile reduces the extent of the separated flow which causes the interaction to shrink and the upstream influence and separation lines to move closer to the compression corner. Reduced loading in the intermittent region is caused by a weaker separation shock. The separation shock also has an enhanced jitter motion which shifts the frequency band of the loads to a higher band which reduces the energy levels in the skin panels' resonant frequency band.

There are several outstanding issues which need to be addressed in future studies. Based on the results of past studies, it has been assumed that the enhanced separation shock jitter is due to increased turbulence. This assumption needs to be verified with turbulence intensity measurements in the incoming boundary layer over the span of the VGs. The changes in the separation shock velocity history also need to be documented to verify that they are reduced in the disturbed interaction. Future studies will also address the effect of the VGs on the fluctuating pressure loads on the ramp.

Acknowledgments

References

1. Bogdonoff, S. M., "Some Experimental Studies of the Separation of Supersonic Turbulent Boundary Layers," Heat Transfer and Fluid Mechanics Institute, UCLA, June 23-25, 1955, sec. V, pp. 1-23.
2. Chapman, D. R., D. M. Kuehn, and H. K. Larson, "Investigation of Separated Flows in Supersonic and Subsonic Streams with Emphasis on the Effect of Transition," NACA Report 1356, 1958.
3. Kistler, A. L., "Fluctuating Wall Pressure under a Separated Supersonic Flow," Journal of the Acoustical Society of America, Vol. 36, No. 3, pp. 543-550.
4. Dolling, D. S., "Fluctuating Loads in Shock Wave Turbulent Boundary Layer Interaction: Tutorial and Update," AIAA Paper 93-0284, Jan. 11-14, 1993, Reno, NV.

5. Pozefsky, P., R. D. Blevins, and A. L. Laganelli, "Thermo- Vibro-Acoustic Loads and Fatigue of Hypersonic Flight Vehicle Structures," AFWAL TR-89-3014, Feb. 1989.

6. Raghunathan, S., "Passive Control of Shock Boundary Layer Interaction," *Progress in Aerospace Sciences*, Vol. 25, No. 3, pp. 271-296, Mar. 1988.

7. Grin, V. T., and N. N. Zakharov, "Experimental Investigation of Effect of Tangential Blowing and Wall Cooling on Flow with Separation," *Fluid Dynamics*, Vol. 6, pp. 1035-1038, Jun. 1974.

8. Viswanath, P. R., L. Sankaran, P. M. Sagdeo, R. Narasimha, and A. Prabhu, "Injection Slot Location for Boundary Layer Control in Shock-Induced Separation," *Journal of Aircraft*, Vol. 20, No. 8, pp. 726-732, Aug. 1983.

9. Ball, K. O. W., and R. H. Korkegi, "An Investigation of the Effect of Suction on Hypersonic Laminar Boundary Layer Separation," *AIAA Journal*, Vol. 6, No. 2, pp. 239-243, Feb. 1968.

10. Viswanath, P. R., "Shock-Wave-Turbulent-Boundary-Layer Interaction and Its Control: A Survey of Recent Developments," <u>Developments in Fluid Mechanics and Space Technology</u>, edited by Narasimha, R., and A. P. J. Abdul Kalam, Indian Academy of Sciences, Bangalore, India, pp. 143-202, 1988.

11. McClure, W. B., "An Experimental Study of the Driving Mechanism and Control of the Unsteady Shock Induced Turbulent Separation in a Mach 5 Compression Corner Flow," Ph.D. Dissertation, Dept. of Aerospace Engineering and Engineering Mechanics, The University of Texas at Austin, Aug. 1992.

12. Kleifges, K. and D. S. Dolling, "Control of Unsteady Shock-Induced Turbulent Boundary Layer Separation Upstream of Blunt Fins," AIAA Paper 93-3281, July 6-9, 1993, Orlando, FL.

13. Wheeler, G. O., "Means for Maintaining Attached Flow of a Flowing Medium," United States Patent #4,455,045.

14. Gartling, D. K, "Tests of Vortex Generators to Prevent Separation of Supersonic Flow in a Compression Corner," Master's of Science Thesis, Dept. of Aerospace Engineering, The University of Texas at Austin, 1971.

15. Pearcey, H. H., (1961) "Shock-Induced Separation and Its Prevention by Design and Boundary Layer Control," *Boundary Layer and Flow Control: Its Principles and Applications*, Vol. 2, edited by G. V. Lachman, Pergamon Press, Inc., New York, 1961.

16. Barber, T. J., J. S. Mounts, and D. C. McCormick, "Boundary Layer Energization by Means of Optimized Vortex Generators," AIAA Paper 93-0445, Jan. 11-14, 1993, Reno, NV.

17. McCormick, D. C., "Shock-Boundary Layer Interaction Control with Low-Profile Vortex Generators and Passive Cavity," AIAA Paper 92-0064, Jan. 6-9, 1992, Reno, NV.

18. Gonsalez, J. C., and D. S. Dolling, "Correlation of Interaction Sweepback Effects on the Dynamics of Shock-Induced Turbulent Separation," AIAA Paper 93-0776, Jan. 11-14, 1993, Reno, NV.

19. Marshall, T. A., and D. S. Dolling, "Spanwise Properties of the Unsteady Separation Shock in a Mach 5 Unswept Compression Ramp Interaction," AIAA Paper 90-0377, Jan. 8-11, 1990, Reno, NV.

20. Brusniak, L., "Evaluation of Conditional Sampling Methods of Analyzing Separation Shock Motion," AIAA Paper 88-0091, Jan. 1988, Reno, NV.

21. Erengil, M. E., and D. S. Dolling, "Unsteady Wave Structure near Separation in a Mach 5 Compression Ramp Interaction," *AIAA Journal*, Vol. 29, No. 5, pp. 728-735, May 1991.

22. Gonsalez, J. C., "Correlation of Interaction Sweepback Effects on Unsteady Shock-Induced Turbulent Separation," Master's Thesis, Dept. of Aerospace Engineering and Engineering Mechanics, The University of Texas at Austin, May 1993.

23. Erengil, M. E., and D. S. Dolling, "Physical Causes of Separation Shock Unsteadiness in Shock Wave/Turbulent Boundary-Layer Interactions," AIAA Paper 93-3134, AIAA 24th Fluid Dynamics Conference, July 6-9, 1993, Orlando, FL.

24. Gramann, R. A., and D. S. Dolling, "Detection of Turbulent Boundary Layer Separation Using Fluctuating Wall Pressure Signals," AIAA Journal, Vol. 28, No. 6, pp. 1052-1056.

25. Erengil, M. E., "Physical Causes of Separation Shock Unsteadiness in Shock Wave/Turbulent Boundary-Layer Interactions," Ph.D. Dissertation, Dept. of Aerospace Engineering and Engineering Mechanics, The University of Texas at Austin, Dec. 1993.

Section 2:

Reduction of Fluctuating Pressure Loads in Shock Wave Turbulent Boundary Layer Interactions

Reduction of Fluctuating Pressure Loads in Shock Wave Turbulent Boundary Layer Interactions

J. W. Barter[*] and D. S. Dolling[+]

Fluctuating surface pressure measurements have been made to investigate the effectiveness of Boundary Layer Separators (BLSs) in reducing the fluctuating pressure loads produced by separated shock wave turbulent boundary layer interactions. Measurements have been made under unswept and swept compression corner interactions in a Mach 5 flow. BLSs fix the separation location and eliminate the large-amplitude, low-frequency fluctuating pressure loads upstream of the compression corners. The loads on the unswept compression corner face are reduced by as much as 59%. The BLSs also shift the mean pressure distribution on the unswept corner face in the streamwise direction. Results show that the loads on the corner face vary with the BLS height and the distance between the BLS and the compression corner. Suggestions for the optimum placement and the use of the BLSs are also made.

Nomenclature

C_f	skin friction coefficient
$G(f)$	spectral density function
L	distance between the leading edge of the compression corner and the trailing edge of the boundary layer separator, normalized by δ
P	mean pressure
Re_δ	Reynolds number based on boundary layer thickness
St	Strouhal number based on U_∞ and the BLS height
T	temperature
U	velocity
X	streamwise distance normalized by δ (fig. 1)
Y	spanwise distance normalized by δ (fig. 1)
Z	vertical distance normalized by δ (fig. 1)
f	frequency
x'	streamwise distance downstream of the BLS
Π	undisturbed boundary layer wake strength parameter
β	fraction of wall pressure variance in the 100-500 Hz. band
δ	undisturbed boundary layer thickness
δ^*	undisturbed boundary layer displacement thickness
η	distance from the leading edge of a swept compression corner, measured normal to the leading edge and positive downstream of it, normalized by δ
λ_c	leading edge sweepback angle
σ	standard deviation
θ	undisturbed boundary layer momentum thickness

---

[*] Graduate Student, Student Member AIAA
[+] Professor, Associate Fellow AIAA

Subscripts:
max   maximum value
o   stagnation quantity
pw   wall pressure
w   wall
∞   freestream condition

Abbreviations:
BLS   boundary layer separator
RMS   root mean squared value
SWTBLI   shock wave/turbulent boundary layer interaction

Introduction

It is well known that when a shock wave of sufficient strength interacts with a boundary layer it can cause separation. In the case of shock-induced turbulent boundary layer separation, high speed cinematography as early as the 1950's[1,2] showed that the process is unsteady. However, due to the lack of adequate instrumentation, most early studies addressed mean flow properties only. Kistler,[3] in 1964, was probably the first to make detailed fluctuating wall pressure measurements under the separated supersonic turbulent boundary layer upstream of a forward facing step. Since Kistler, there has been an increasing number of studies focusing on interaction unsteadiness. The qualitative character and quantitative details of the unsteadiness naturally vary from one flow type to another, but typically the unsteadiness manifests itself as a large-scale, low-frequency pulsation of the separated flow and flapping of the outgoing boundary layer. A recent review of much of this work has been compiled by Dolling.[4]

Interaction unsteadiness produces large amplitude fluctuating pressure loads as high as 185 dB which can substantially shorten the fatigue life of vehicle components. These high loads occur near separation and reattachment, and under the outgoing boundary layer, and are caused by fluctuations in the instantaneous positions of separation and reattachment. The frequency band of the highest amplitude loads is typically in the range of several hundred Hz to several kHz, which exacerbates the loading problem because the typical resonant frequency band for skin panels is 100-500 Hz. Predictions by Pozefsky, et al.[5] for a transatmospheric vehicle suggest that the time to failure of metal matrix composite structures under such loading is typically on the order of minutes.

The region of separated flow produced by shock wave turbulent boundary layer interactions can also substantially reduce aerodynamic efficiency. Consequently, many previous attempts to control these interactions have focused on either eliminating separation or reducing the total pressure loss through the interaction.[6-10] In light of the effect of shock wave turbulent boundary layer interactions on structural fatigue, some recent control studies have focused on loads reduction. McClure[11] explored a number of techniques, including Boundary Layer Manipulators and riblets, with limited success. Kleifges and Dolling[12] had greater success using a swept root fillet to reduce the loads produced in an unswept blunt fin induced interaction. Barter and Dolling[13] had reasonable success using vortex generators to control the loads produced by unswept compression corner interactions.

The objective of the current study is to explore ways to reduce fluctuating pressure loads in shock wave turbulent boundary layer interactions to extend fatigue life. It is hoped that through changes in the separation shock dynamics (and reattachment process), the magnitude of the loading can be reduced, its spectral content altered, and the area exposed to high loads reduced. In the study reported in this paper, the effects of Boundary Layer Separators (BLSs) are examined.

To the authors' knowledge this control technique has never been investigated. The idea behind this concept is relatively simple. Since the fluctuating pressure loads through the interaction are largely the result of separation and reattachment unsteadiness, one way to reduce the loads is to reduce or eliminate this unsteadiness. The BLS forces the boundary layer to separate at a fixed location thus eliminating the separation shock unsteadiness. By eliminating the separation shock unsteadiness, low-frequency pressure fluctuations upstream of the compression corner should largely disappear. While fixing the separation point will not fix the reattachment location, it is hoped that the amplitude of the reattachment unsteadiness may be reduced thereby reducing the loads on the corner face.

2

Experimental Program

Wind Tunnel and Flow Conditions

All experiments were conducted in the Mach 5 blowdown wind tunnel at The University of Texas at Austin. The air supply for this tunnel is stored in tanks with a combined volume of 140 ft.^{3} (3.96 m^3) at a maximum pressure of 2500 psig. (17.3 MPa). Maximum run times are about a minute. A computer controlled valve regulates the flow of air from the tanks to the settling chamber such that a constant stagnation pressure (to within ±1.5%) is maintained. Two banks of 420 kW nichrome wire heaters raise the temperature of the air in the settling chamber to the desired value.

Parameter		
M_∞	4.92	4.92
P_0	340 psia.	2.34 MPa
T_0	640° R	356 K
U_∞	2530 ft/s	770 m/s
δ	0.76 in.	1.93 cm
Re_δ	1.29 x 10^6	1.29 x 10^6
δ^*	0.36 in.	0.90 cm
θ	0.030 in.	0.075 cm
C_f x 10^3	0.76	0.76
Π	0.44	0.44

Table 1: Freestream Flow Conditions and Undisturbed Turbulent Boundary Layer Properties

The test section used for these experiments is 27 in. (68.6 cm) long, 6 in. (15.2 cm) wide and 7 in. (17.8 cm) high. All tests were conducted with the models mounted on the test section floor. The floor boundary layer undergoes natural transition upstream of the nozzle and develops under approximately adiabatic wall temperature conditions. Values of the stagnation and freestream properties, and undisturbed boundary layer parameters measured approximately 1δ upstream of the compression corner
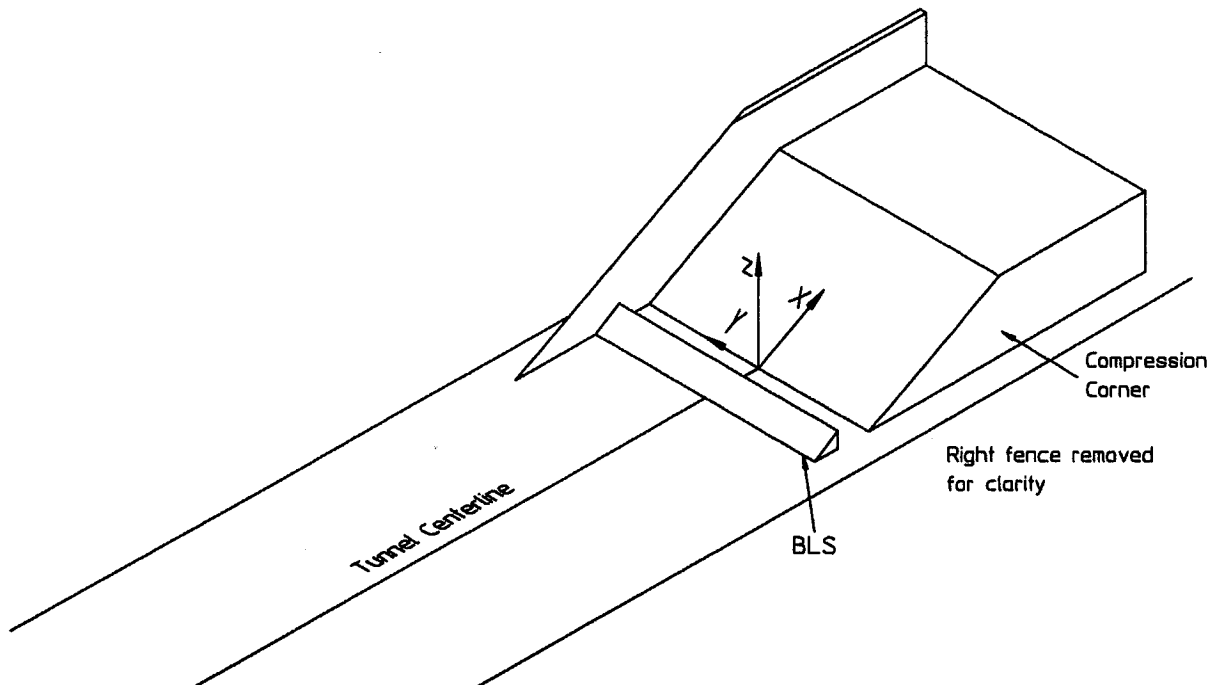

Figure 1: 28 Degree Unswept Compression Corner Model with BLS Upstream

location are listed in Table 1.

Models

The majority of this study focuses on the effect of the BLSs on a SWTBLI induced by a 28° unswept compression corner. This particular interaction was selected because it produces a nominally two-dimensional flowfield that has been studied in detail in this facility.[11,14,15] The model is 6.25δ wide and 1.97δ high and it can be adjusted streamwise relative to fixed transducers upstream. This model, with a BLS upstream, is shown in Figure 1. Fences, 0.16δ thick, were attached to the model to prevent spillage and to isolate it from the tunnel side-wall boundary layers. The leading edges of the fences were beveled to prevent shocks from interfering with the interaction. The fences extended 3.95δ upstream of, and 1.32δ above the compression corner model.

A second 28° unswept compression corner model was used to assess the effects of the BLSs on the corner face loads. This model has transducer ports along its centerline and can be slid out of the tunnel floor to provide greater flexibility in positioning the transducers relative to the corner line. This model is 4.61δ wide and 2.37δ high. Beveled, 0.25δ thick fences were attached to the sides of the model and extended 3.95δ upstream of and 1.32δ above the compression corner model.

To assess the applicability of this control technique to swept compression corner induced interactions, a BLS was placed upstream of two different swept corners. Both corners have 28° streamwise angles. The first swept corner had a corner line sweepback angle of 20° (λ_c=20). This model is 1.97δ high and 6.58δ wide and had a 0.12δ thick, beveled fence attached at its apex. The fence extended 0.99δ above and 4.28δ upstream of the model. The second swept corner, λ_c=30, is 2.63δ high and 5.59δ wide, and had a 0.12δ thick, beveled fence attached at its apex. The fence extended 0.99δ above and 3.95δ upstream of the model.

Three different BLSs were primarily used for this study. These BLSs are shaped like small wedges as shown in Figure 1 and were attached to the tunnel floor using super-glue. Their dimensions are given in Table 2 along with the dimensions of the 0.4x0.2 block-shaped BLS that was used in a later phase of this study. When the BLSs were placed upstream of the unswept compression corners, they spanned the distance between the fences thus preserving the nominal two-dimensionality of the flow. When they were placed upstream of the swept compression corners, the edge of the BLS next to the fence was cut such that the BLS was flush with the fence. The BLS was mounted parallel to the leading edge of the corner and extended 6.25δ from the fence (measured parallel to the corner leading edge).

BLS	Height/δ	Length/δ
0.8x0.2	0.24	1.06
0.4x0.2	0.26	0.53
0.4x0.1	0.13	0.52
0.4x0.2 block	0.26	0.53

Table 2: BLS Dimensions

Instrumentation and Data Acquisition

Wall pressure measurements were made using Kulite model XCQ-062-15A (0-15 psia.) and XCQ-062-50A (0-50 psia.) transducers. The outside diameter of these transducers is nominally 0.0625 in. (0.16 cm). The pressure sensing element is a 0.028 in. (0.071 cm) diameter silicon diaphragm with a Wheatstone bridge atomically diffused into it. With their protective screens in place, these transducers have a frequency response of about 50 kHz when mounted flush with the tunnel wall. They were installed in a 3.375 in. (8.57 cm) diameter circular plug that could be inserted flush with the tunnel floor. When transducer ports were not being used, they were filled with dummy plugs. To insure that the transducers and dummy plugs were flush with the plug face, the installation was inspected using a magnifying glass. The plug could be rotated such that the row of transducers was at any angle relative to the incoming flow. The interaction produced by the unswept compression corner is nominally two-dimensional; therefore, it was investigated using a single streamwise row of transducers placed along the

4

tunnel centerline. Interactions produced by the swept compression corners were investigated with a row of transducers oriented normal to the corner leading edge.

The output of the transducers was amplified and low-pass filtered at a cut-off frequency of 50 kHz. to prevent aliasing. The transducers were statically calibrated daily. During the calibration procedure the amplifier bias and gain were set so that the amplified output would span the entire 0-4.096 V range of the A/D converter. The maximum amplitude of the electronic noise at the input to the A/D converter was less than 10 mV corresponding to a typical signal to noise ratio of about 100. The LeCroy 6810 Waveform Recorder employs a 12-bit A/D converter and was operated at a sampling frequency of 200 kHz/channel. During a typical run, eight channels of data were sampled simultaneously with 512 records (1024 points/record) of data acquired per channel.

Data Analysis

The basic statistical properties of the data (mean, standard deviation, etc.) were computed along with the autocorrelation and cross-correlations between different channels. To evaluate the BLSs' effectiveness in shifting the energy of the wall pressure fluctuations to a higher frequency band it is necessary to quantify the fraction of the overall variance in a given frequency band. The spectral density function, $G(f)$, describes how the mean squared value of the wall pressure is distributed in the frequency domain. The integral of $G(f)$ over a prescribed frequency band divided by the overall variance of the wall pressure gives the fraction of energy, β, due to wall pressure fluctuations in the frequency band (equation 1). According to Pozefsky, et al.,[5] the typical resonant frequency band for aircraft skin panels is 100-500 Hz. The above technique is used to determine the effectiveness of the VGs in decreasing β with respect to this frequency band.

where

$$\beta = \frac{\int_{f_{min}}^{f_{max}} G(f)\, df}{\sigma^2}$$

(1)

$$\sigma^2 = \int_0^\infty G(f)\, df$$

Results

<u>Undisturbed Interaction</u>

The separation shock motion in SWTBLIs has been characterized by Erengil and Dolling as having two components.[14] The first is a low-amplitude, high frequency jitter motion produced by fluctuations in the instantaneous pressure ratio across the separation shock. This jitter is superimposed upon a large-scale, low-frequency motion produced by pulsation of the separated flow. The combination of these two types of motion produces the observed streamwise variation in the flow properties.
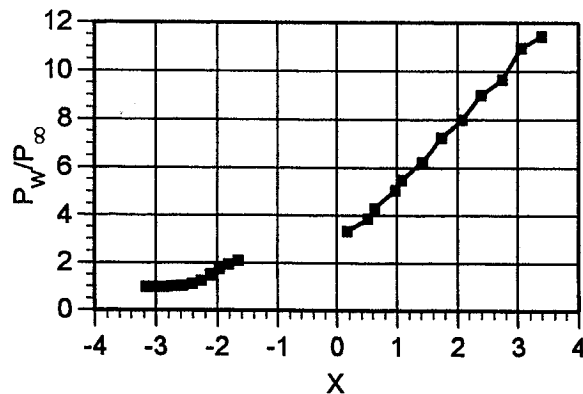

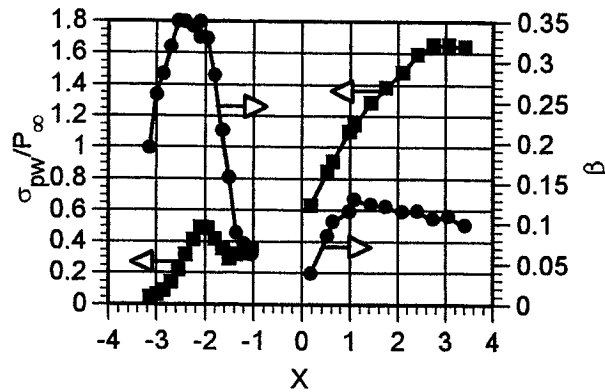Figure 2: Mean Wall Pressure Distribution Through the Undisturbed Interaction

Figure 3: Wall Pressure RMS and β Distributions Through the Undisturbed Interaction

The mean wall pressure distribution through the unswept compression corner induced interaction is shown in Figure 2 and the wall pressure RMS and the β distributions are shown in Figure 3. The intermittent region (i.e., the region of separation shock motion) is 1.4δ long with upstream influence (i.e., the furthest upstream point of separation shock travel) located 2.9δ upstream of the compression corner leading edge. The maximum wall pressure RMS upstream of the compression corner, nondimensionalized by P_∞, is 0.48. The maximum fraction of energy in the structural resonant frequency band, β, occurs upstream of the corner and has a magnitude of 0.35. For a better understanding of the loads in the intermittent region of the undisturbed interaction, the reader is referred to Barter and Dolling[13].

Downstream of reattachment on the compression corner face, the mean pressure rises to a pressure ratio of about 12 which is the pressure ratio predicted by inviscid shock theory for this turning angle. The inviscid pressure ratio is not achieved because the corner face is too short. Unsteadiness in the reattachment process and compression of the outgoing boundary layer produce high fluctuating pressure loads on the corner face ($\sigma_{pw,max}/P_\infty = 1.65$) with 10-13% of the fluctuation energy contained in the structural resonant frequency band.
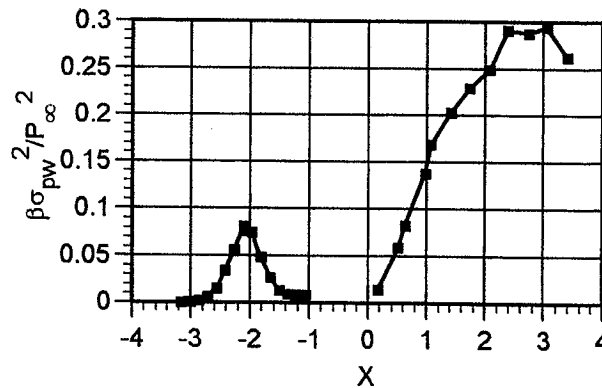

Figure 4: Distribution of Wall Pressure Variance in the Structural Resonant Frequency Band for the Undisturbed Interaction

Figure 4 shows the distribution of the wall pressure variance in the structural resonant frequency band through the undisturbed interaction. This figure shows how β and σ_{pw} influence the amount of energy in the structural resonant frequency band. Upstream of the compression corner where β is high (compared to the corner face) but σ_{pw} is low, the wall pressure variance in the resonant band is low. However, on the compression corner face where σ_{pw} increases dramatically the amount of energy in the resonant band increases sharply despite a reduced β.

6

<u>Effects of the BLSs on the Flowfield</u>

Use of the BLS, as its name suggests, allows one to control separation. For the range of BLS locations tested, it was found that BLSs with leading edge angles less than that needed for incipient separation have no separation upstream of the BLS and there is an attached shock located at its leading edge. For BLSs with angles greater than incipient separation (such as the 0.4x0.2 BLS), separation occurs upstream of the BLS. The flow field upstream of the BLSs is similar to the undisturbed interaction but of much smaller scale. That is, there is an unsteady separation shock upstream of the BLS followed by a separation bubble. However, since the scale of the interaction is smaller the loads are lower and the amount of energy in the structural resonant frequency band is less than in the undisturbed interaction. It is noteworthy that the qualitative effects of the BLSs on the flow field are independent of the BLS location over the range tested ($3.05 \leq L \leq 0.95$).

Downstream of the BLS is a region of separated flow spanned by a shear layer. The shear layer extends from the trailing edge of the BLS to the compression corner face where it reattaches. Figure 5 shows the evolution of the wall pressure power spectrum downstream of the 0.8x0.2 BLS. Immediately downstream of the BLS (Figure 5a), the power spectrum shows significant energy in the structural resonant frequency band. Within 0.55δ downstream of the BLS this low-frequency energy has decreased substantially (Figure 5b). Moreover, it can be seen in Figure 5b that most of the wall pressure fluctuation energy is contained in a narrow band (as compared to an equilibrium turbulent boundary spectrum) centered at about 20 kHz. This narrow band of energy is also apparent in Figure 5a and is the dominant feature of the spectra up to the reattachment location of the shear layer (Figure 5c). Beyond
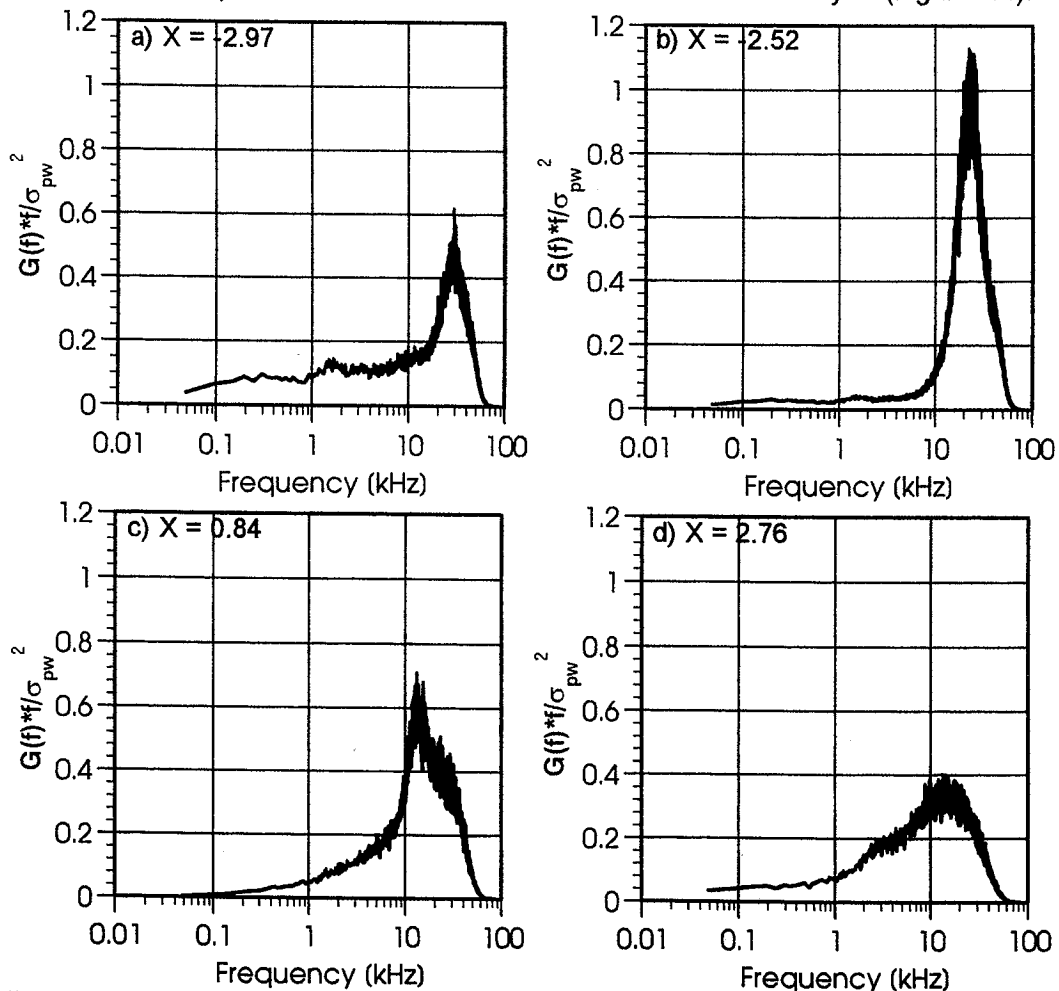

Figure 5: Normalized Wall Pressure Power Spectra Measured Under the Separated Flow Downstream of the 0.8x 0.2 BLS with L=3.05

reattachment, the spectra (Figure 5d) take on a form similar to that measured under the reattached boundary layer in the undisturbed interaction.

Autocorrelations (not shown) of the pressure fluctuations measured between the BLS and reattachment as well as visual inspection of the raw data show clearly the periodicity of the pressure fluctuations in this region. It is well known that the autocorrelation of a sine wave is itself a sine wave. The autocorrelations of the pressure fluctuations have a damped sinusoidal behavior with a period that is consistent with the frequency band indicated in the spectra. The frequency suggested by autocorrelation periodicity is defined as the center frequency.
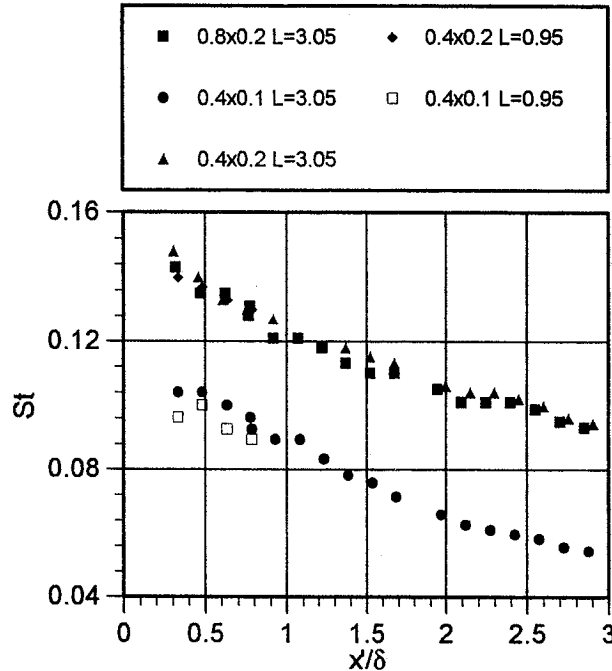
Figure 6: Wall Pressure Fluctuation Center Frequencies Downstream of the BLSs

The center frequency of the narrow band fluctuations downstream of the BLS varies with the streamwise position and BLS height. Figure 6 shows the streamwise variation of the center frequency in terms of a Strouhal number based on the BLS height and the freestream velocity. It can be seen that the Strouhal number for a given height decreases in the downstream direction and the results are independent of L. Note that the separation upstream of the 0.4x0.2 BLS has no effect on the frequencies of the pressure fluctuations downstream of it. The 0.4x0.1 BLS produces higher center frequencies at a given streamwise position than observed for the 0.8x0.2 and 0.4x0.2 BLSs; however, the increase in frequency is not proportional to the decrease in height of the BLS. As a result, the use of the height as a normalizing parameter fails to collapse the data. The cause of these narrow-band, high-frequency fluctuations is not well understood at this time. It is hoped that future research will resolve the cause and scaling of these fluctuations.

Effect of BLS on Fluctuating Pressure Loads in Unswept Interactions

I. BLSs Placed Upstream of the Undisturbed Intermittent Region

Placement of the BLSs upstream of the interaction dramatically affects the loads through the interaction and can be used to change the mean pressure distribution on the corner face. Figure 7 shows mean pressure distributions for the undisturbed interaction and when the BLSs have been placed 3.05δ upstream of the compression corner. At this BLS location, the BLS trailing edge is slightly upstream of the upstream influence of the undisturbed interaction. There is some scatter in the data taken between the BLS and the compression corner due to different bias errors for each transducer but in essence the mean pressure in this region is nearly constant. The pressure gradient on the compression corner face is

8

essentially the same for the four cases shown. However, each distribution is shifted downstream (relative to the undisturbed interaction) due to variations in the reattachment location. Reattachment for all three BLS cases is downstream of the reattachment location in the undisturbed interaction. It is also evident in this figure that the BLS height but not the BLS's leading edge angle is an important parameter. The cases that have the same BLS height (0.8x0.2 and 0.4x0.2) produce pressure distributions on the ramp face that essentially are the same.

Placement of the BLSs upstream of the corner reduces the magnitude of the loads upstream of the corner and on the corner face as seen in Figure 8. Since the BLS fixes separation, the local maximum in the wall pressure RMS distribution upstream of the corner for the undisturbed interaction is eliminated. The wall pressure RMS rises monotonically from the trailing edge of the BLS to the leading edge of the corner and reaches levels at the corner leading edge that are as high as those found in the undisturbed interaction.
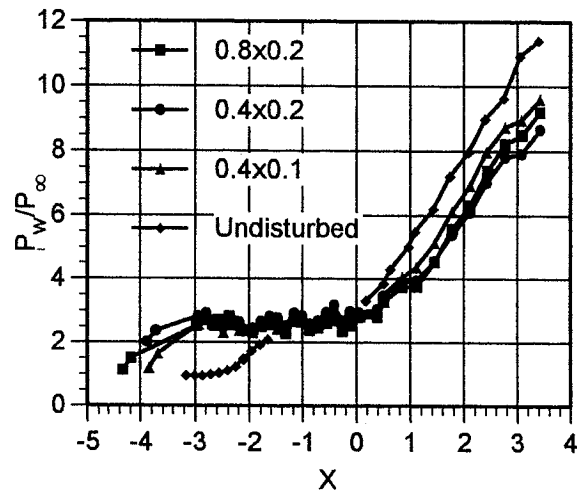
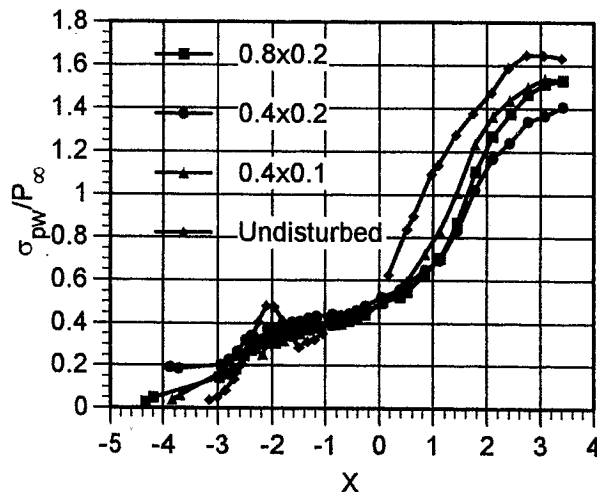Figure 7: Mean Wall Pressure Distributions with BLSs Upstream and L=3.05

Figure 8: Wall Pressure RMS Distributions with BLSs Upstream and L=3.05

Downstream of the corner leading edge the BLSs reduce the loads compared to the undisturbed interaction. The loads on the ramp face are largely the result of reattachment unsteadiness.[16] This reduction in the corner face loads is the result of lower amplitude fluctuations in the instantaneous reattachment location. Table 3 shows the maximum loads for each of the BLS cases. As a result of the BLSs, loads on the corner face are reduced by up to 15%. For each of these BLS cases, the highest

loads occurred at the last station on the corner face; therefore, the largest loads for each of these cases may be higher than reported here.

The BLSs also reduce the fraction of the total wall pressure fluctuation energy contained in the structural resonant frequency band as shown in Figure 9. The BLSs reduce β upstream of the corner by eliminating the large-scale unsteadiness present in the undisturbed interaction. Similarly on the compression corner face, β is reduced by reducing the scale of reattachment unsteadiness. It is noteworthy that despite the separation upstream of it, the 0.4x0.2 BLS has the lowest β_{max} and $\sigma_{pw,max}$ of the BLSs tested. This result is attributed to the 0.4x0.2 BLS preventing interaction between the separation and reattachment processes.

BLS	$(\sigma_p/P_\infty)_{max}$	% Reduction
Undisturbed	1.65	--
0.8x0.2	1.53	7
0.4x0.2	1.41	15
0.4x0.1	1.54	7

Table 3: Effect of the BLSs on the Maximum Wall Pressure RMS for L=3.05
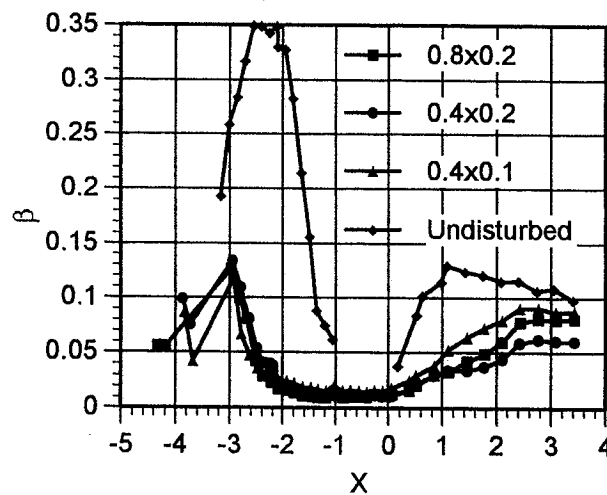

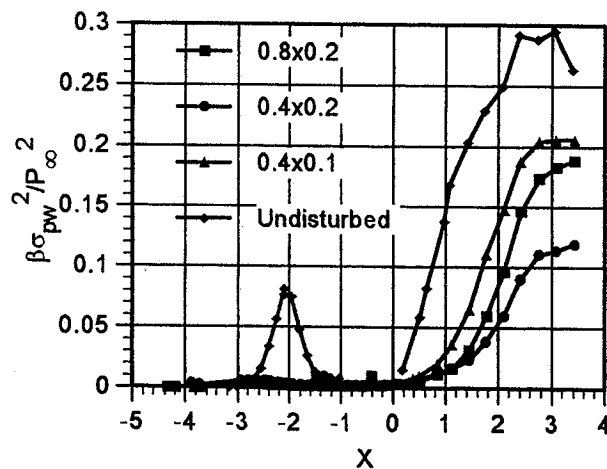Figure 9: β Distributions with BLSs Upstream and L=3.05

Figure 10: Wall Pressure Variance Distributions with BLSs Upstream and L=3.05

As a result of the reductions in β and σ_{pw} the wall pressure fluctuation energy in the structural resonant frequency band is significantly reduced. Figure 10 shows the wall pressure variance in the

resonant band through the disturbed interactions. As it can be seen in this figure, upstream of the corner, energy in the resonant band is virtually eliminated and downstream of the corner leading edge it is significantly reduced. Use of the BLSs reduces the maximum wall pressure variance by up to 59% (Table 4) with the maximum reduction occurring for the 0.4x0.2 BLS.

BLS	$(\beta\sigma_p^2/P_\infty^2)_{max}$	% Reduction
Undisturbed	0.30	--
0.8x0.2	0.19	36
0.4x0.2	0.12	59
0.4x0.1	0.21	30

Table 4: Reduction of Wall Pressure Fluctuation Energy with the BLSs at L=3.05

II. BLSs Placed Downstream of the Undisturbed Intermittent Region

The BLSs were also placed with the BLS leading edge downstream of the downstream end of the intermittent region of the undisturbed interaction. This corresponded to L = 0.95 for the 0.4x0.1 and 0.4x0.2 BLSs and L = 0.42 for the 0.8x0.2 BLS. Mean pressure distributions for these BLS positions are shown in Figure 11. In this case the mean pressure distributions are nearly identical to or steeper than of that of the undisturbed interaction. This indicates that reattachment for these cases occurs upstream of or near the reattachment location of the undisturbed interaction. However, the distributions from cases having the same height (i.e., 0.4x0.2 and 0.8x0.2) do not overlay each other as they did in Figure 7 for the upstream BLS locations. This discrepancy will be discussed later with the data that explains it.
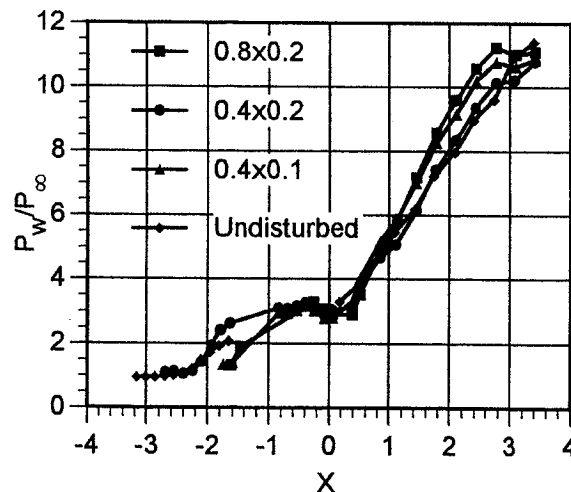

Figure 11: Mean Wall Pressure Distributions with BLSs Upstream and L=0.95 (0.4x0.2 and 0.4x0.1 BLSs) or L=0.42 (0.8x0.2 BLS)

The BLSs affect the wall pressure RMS distribution on the compression corner face favorably. The distributions, shown in Figure 12, show that the maximum RMS is reduced and the distributions on the ramp face for the disturbed cases roll off more rapidly than the undisturbed case. Also note that there is no separation upstream of the 0.8x0.2 and 0.4x0.1 BLSs. The reduced maximum RMS on the corner face, tabulated in Table 5, is obviously beneficial and the rapid roll off is also beneficial because it means that the surface area exposed to the highest loads is reduced by using the BLSs. Like the cases with the BLS placed upstream of upstream influence, there is no correlation between the BLS geometry and the loads on corner face. However, like the previous cases, the use of the 0.4x0.2 BLS results in the smallest loads on the compression corner face despite the separation upstream of it.

The BLSs placed downstream of separation also have a large effect on the frequency content of the wall pressure fluctuations as shown in Figure 13. Upstream of the compression corner, β is reduced because the large-scale separation unsteadiness has been eliminated for the 0.8x0.2 and 0.4x0.1 BLSs and significantly reduced for the 0.4x0.2 BLS. On the corner face β is reduced as compared to values

measured in the undisturbed interaction due to changes in the reattachment dynamics. The 0.4x0.2 BLS produces the lowest βs on the compression corner face.
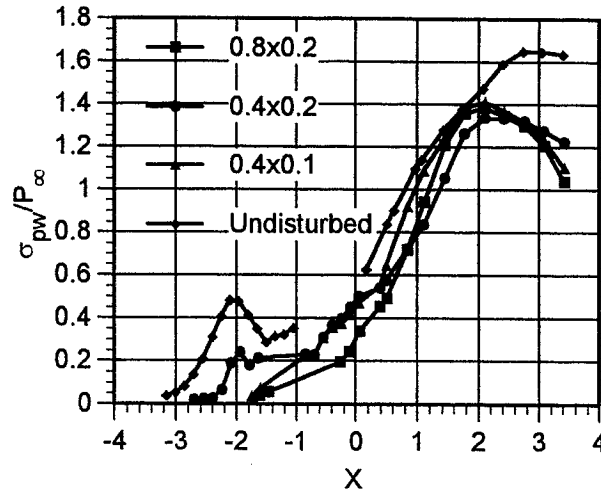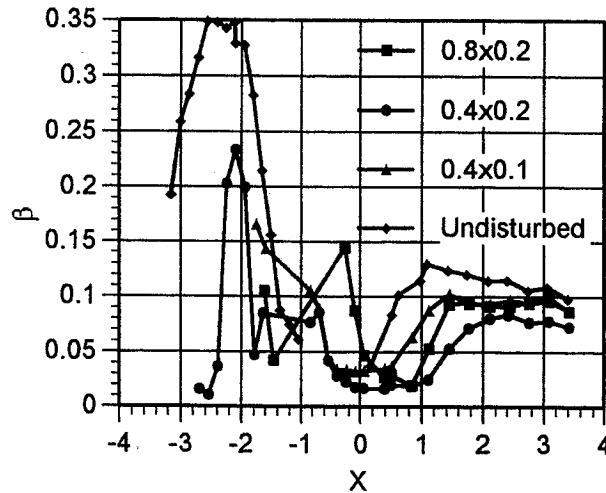

Figure 12: Wall Pressure RMS Distributions with BLSs Upstream and L=0.95 (0.4x0.2 and 0.4x0.1 BLSs) or L=0.42 (0.8x0.2 BLS)

BLS	$(\sigma_p/P_\infty)_{max}$	% Reduction
Undisturbed	1.65	--
0.8x0.2	1.39	16
0.4x0.2	1.34	19
0.4x0.1	1.41	15

Table 5: Maximum Wall Pressure RMSs with BLSs Upstream and L=0.95 (0.4x0.2 and 0.4x0.1 BLSs) and L=0.42 (0.8x0.2 BLS)

Figure 13: β Distributions with BLSs Upstream and L=0.95 (0.4x0.2 and 0.4x0.1 BLSs) or L=0.42 (0.8x0.2 BLS)

The combined effect of the reduction in wall pressure RMS and β levels through the interaction results in significant reduction in the amount of energy in the structural resonant frequency band (Figure 14). Upstream of the corner leading edge there is virtually no energy in the resonant band. On the corner face the maximum energy is reduced by up to 50% (Table 6) and the high energy levels roll off

faster than in the undisturbed interaction. Like the cases where the BLSs were placed upstream of the upstream influence line, the lowest energy levels on the corner face were obtained with the 0.4x0.2 BLS.
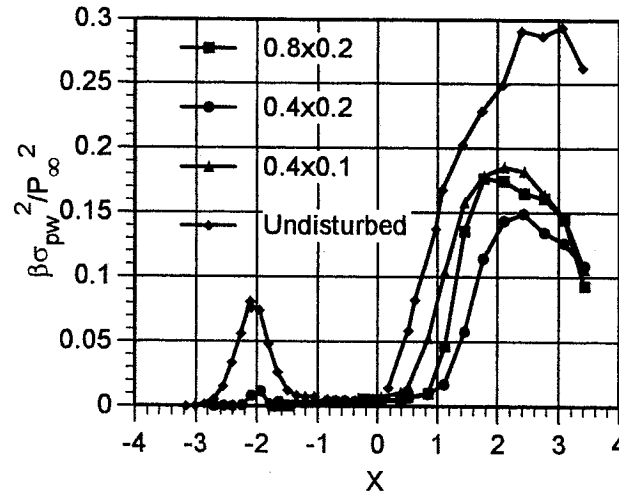

Figure 14: Wall Pressure Variance Distributions with BLSs Upstream and L=0.95 (0.4x0.2 and 0.4x0.1 BLSs) or L=0.42 (0.8x0.2 BLS)

BLS	$(\beta\sigma_p^2/P_\infty^2)_{max}$	% Reduction
Undisturbed	0.30	--
0.8x0.2	0.18	40
0.4x0.2	0.15	50
0.4x0.1	0.19	37

Table 6: Reduction of Wall Pressure Fluctuation Energy with the BLSs at L=0.95 (0.4x0.2 and 0.4x0.1 BLSs) or L=0.42 (0.8x0.2 BLS)

III. Effect of BLS Geometry and Position on the Loads

The above results have shown that the BLS height and L have a fundamental effect on the impact of the BLSs on the interaction. When the 0.8x0.2 and 0.4x0.2 BLSs were placed at L=3.05, the resultant mean pressure distributions on the corner face overlay each other. However, when these two BLSs were placed downstream of separation so that L was different for each BLS, their mean pressure distributions were different.
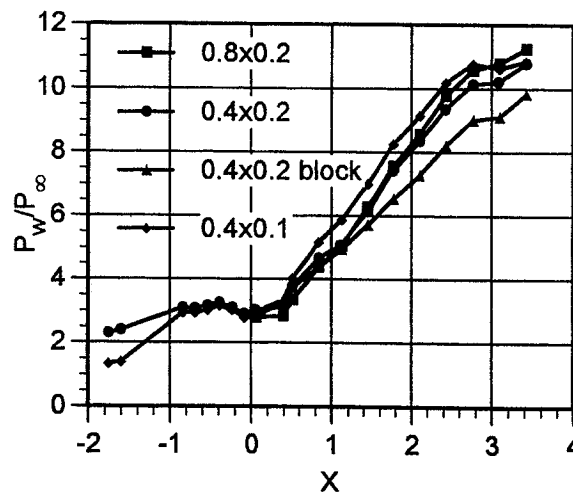

Figure 15: Mean Wall Pressure Distributions with BLSs Upstream and L=0.95

13

To further explore the relationship between the BLS height, L, and BLS shape additional experiments were conducted with the 0.8x0.2 BLS and the 0.4x0.2 block-shaped BLS placed at L=0.95. Results from these experiments are shown in Figures 15-18. Mean pressure distributions shown in Figure 15 are as expected. The 0.4x0.1 BLS reattaches at the lowest point on the compression corner face and therefore its mean pressure distribution is shifted the furthest upstream. The 0.4x0.2 and 0.8x0.2 BLSs have essentially the same reattachment location and therefore their distributions overlay each other. The 0.4x0.2 block BLS is a completely different shape so its mean pressure distribution does not overlay that of the 0.4x0.2 and 0.8x0.2 BLSs.

From the results thus far discussed in this paper, several conclusions about dependence of the reattachment location on the BLS geometry and location can be made. First, the reattachment location is weakly dependent on the BLS shape. If the BLSs have similar shapes, like the 0.4x0.2 and 0.8x0.2 wedge-shaped BLS, then they have essentially the same reattachment location and will produce the same mean pressure distribution on the corner face. However, large changes in the BLS shape such as that between wedge-shaped and block-shaped BLS, have a large effect on the mean pressure distribution on the compression corner face.

Second, the reattachment location is strongly dependent on the BLS height and the distance between the BLS trailing edge and the corner leading edge. Obviously, the shorter the BLS, the lower that reattachment occurs on the corner face. The dependence on L results from the shear layer not being parallel to the tunnel floor. The layer has a small velocity in the positive Z direction. As a result, as L increases, the reattachment location moves downstream on the corner face. Though both L and the BLS height strongly affect the reattachment location, they have no effect on the pressure gradient along the corner face unless reattachment is sufficiently close to the corner leading edge, in which case the gradient becomes steeper.

Figures 8 and 16 show that small changes in the BLS geometry account for almost a 10% variation in the maximum loads on the compression corner face (ignoring the 0.4x0.2 block results). The distance between the BLS trailing edge and the corner leading edge also affects the face loads. As L is reduced from 3.05 to 0.95, $\sigma_{pw,max}$ is reduced by 7%, 4%, and 8% for the 0.8x0.2, 0.4x0.2, 0.4x0.1 BLSs respectively. The greater effect of L is on the roll-off of the high RMS levels on the corner face. With the BLSs placed at L=3.05, the maximum RMS has a broad peak and doesn't begin to roll-off until after X = 3.4 However, with the BLSs placed at L = 0.95, the roll-off occurs at about X = 2.4 thereby reducing the surface area exposed to the highest loads on the corner face. Regarding this result a word of caution is warranted. The instrumented compression corner model used in this experiment was too short to observe the beginning of the RMS roll-off for the cases where the BLSs were placed at L=3.05. Therefore, the actual $\sigma_{pw,max}$ reported for these cases may be higher and L may have a greater effect on $\sigma_{pw,max}$ than reported.
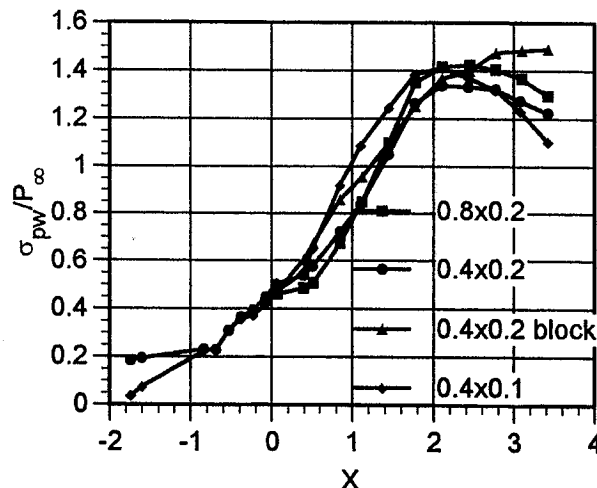

Figure 16: Wall Pressure RMS Distributions with BLSs Upstream and L=0.95

14

Figures 9 and 17 show how the frequency content of the wall pressure fluctuations are affected by changes in the BLS geometry and L. Moving the BLSs downstream causes a small increase in β. The most interesting result is that the 0.4x0.2 wedge-shaped BLS consistently produces the lowest βs on the compression corner face. Furthermore, the 0.4x0.2 block-shaped BLS produces essentially the same βs on the compression corner face as the 0.4x0.1 and 0.8x0.2 BLSs.
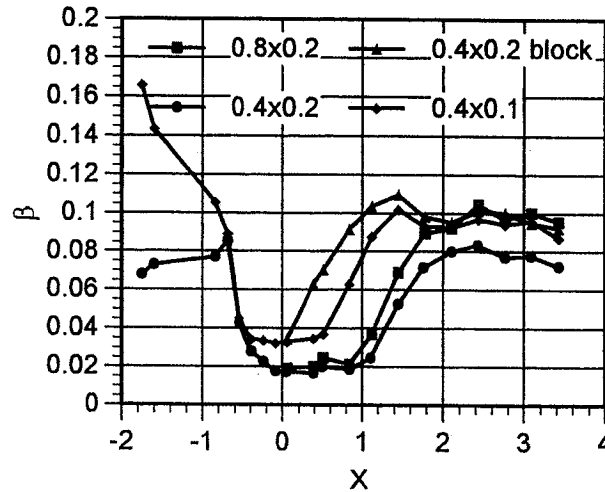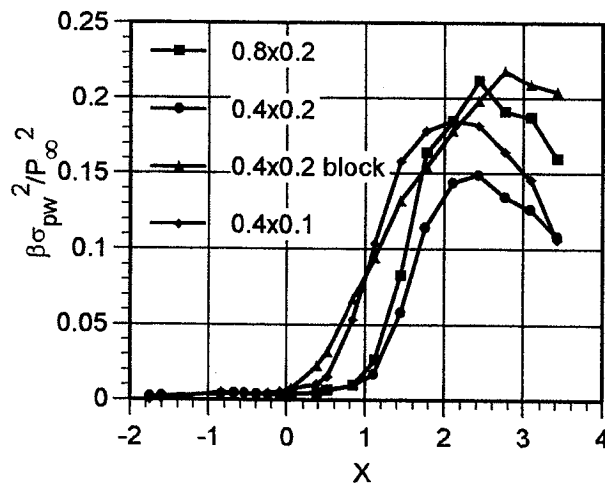

Figure 17: β Distributions with BLSs Upstream and L=0.95

Figure 18: Wall Pressure Variance Distributions with BLSs Upstream and L=0.95

While the BLS geometry and L have only a small effect on σ_{pw} and β, their combined effect is significant. The net effect of the BLSs on the energy of the wall pressure fluctuations with frequencies in the structural resonant frequency band is shown in Figures 10 and 18. The differences in the loads on the compression corner face as L, BLS height, and the BLS shape change are attributed to differences in the reattachment dynamics. With the BLSs placed at L=3.05 the maximum energy reduction is 59% with the 0.4x0.2 wedge-shaped BLS but with L=0.95 the maximum energy reduction is only 50%. The results in these two Figures do show that the BLS shape, height, and L significantly affect the amount of energy in the resonant band. Also note that the 0.4x0.2 wedge-shaped BLS consistently produces the lowest energy levels on the corner face.

IV. Implications of the Results on the Implementation of BLS Control

The results discussed above present some interesting options for designers attempting to use this control technique. By placing the BLS close to the compression corner leading edge, the integral of the

mean pressure over the compression corner face can be increased for a fixed control surface length. For applications such as an aileron, the same control effectiveness with either a shorter control surface or smaller deflection angle can be achieved. Using a smaller deflection angle would further decrease the loads on the face. Shortening the surface may make it possible to achieve the same control effectiveness without making the panel so long that it is exposed to the highest energy loads.

An added benefit of placing the BLSs close to the corner leading edge is that this location is also the location where the energy in the resonant band is reduced the most for BLSs with no separation upstream of them. However, designers may also consider using a blunter BLS (i.e. one with separation upstream of it) and moving it further upstream. In this study, it was found that the 0.4x0.2 BLS placed at L = 3.05 reduces the maximum energy in the resonant band by 59% as compared to a 40% reduction for the 0.8x0.2 BLS placed at L = 0.95. However, the additional reduction provided by the 0.4x0.2 BLS comes at the cost of separation upstream of it which results in higher loads upstream of the blunter BLS than are observed upstream of the other BLSs.

Effect of BLSs on the Fluctuating Pressure Loads in Swept Interactions

The 0.8x0.2 BLS was placed 0.95δ upstream of the two swept compression corner models and parallel to the corner leading edge. The transducers were installed normal to the compression corner leading edge. For the corner with λ_c=20° the transducers were 4.54δ from the apex and for the λ_c=30° corner the transducers were 3.91δ from the apex (measured parallel to the corner leading edge).
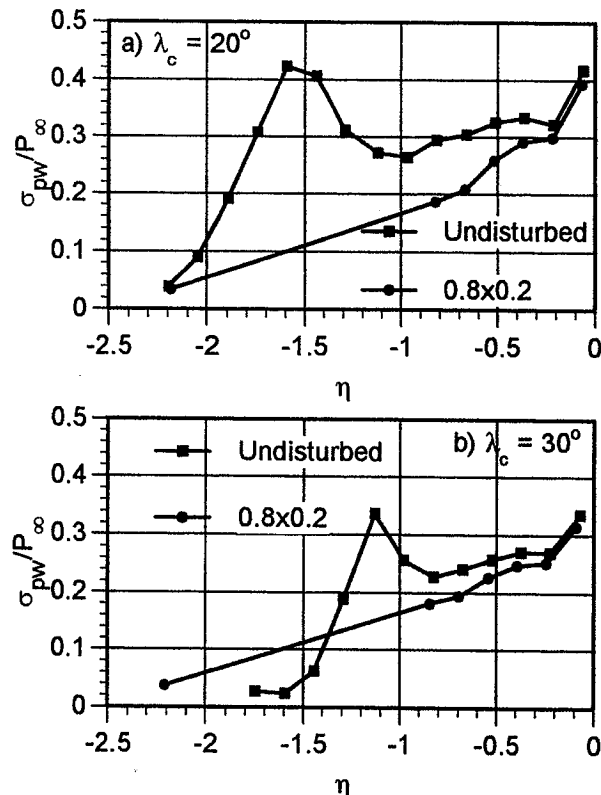

Figure 19: Wall Pressure RMS Distributions Upstream of Swept Compression Corners a) λ_c = 20°, b) λ_c = 30°

Mean pressure measurements upstream of the corner (not shown) show that there is no separation upstream of the BLS for both interactions. Wall pressure RMS distributions shown in Figure 19 demonstrate that for each interaction, the BLS eliminated the local maximum in the undisturbed distribution associated with unsteady separation shock motion. However, downstream of the BLSs the loading levels rise and at the leading edges of the corners (η=0), the loads are essentially the same for the undisturbed and disturbed interactions.

16

Beta distributions upstream of the swept compression corners, shown in Figure 20, demonstrate that the BLSs also eliminate the low-frequency wall pressure fluctuation energy in the structural resonant frequency band. The local maximum in the undisturbed β distributions is associated with the unsteady separation shock and is eliminated by the BLSs. Near the compression corner leading edge, β is essentially the same for the undisturbed and disturbed interactions.

The net effect of the BLSs on the loads in structural resonant frequency band is shown in Figure 21. It can be seen that due to the elimination of the unsteady separation shock, there is essentially no energy in the resonant band. Near the corner leading edge, the energy levels are about the same in both the undisturbed and disturbed interactions.
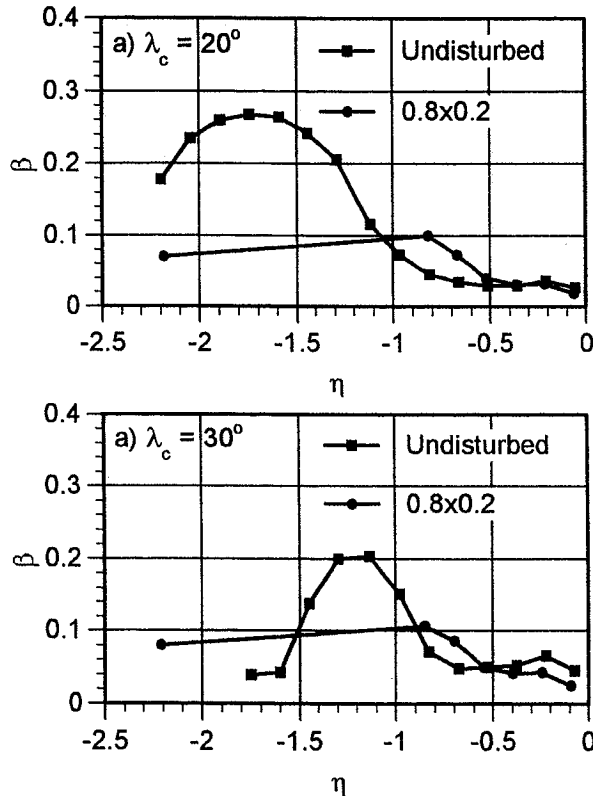
Figure 20: Wall Pressure β Distributions Upstream of Swept Compression Corners a) $\lambda_c = 20°$, b) $\lambda_c = 30°$
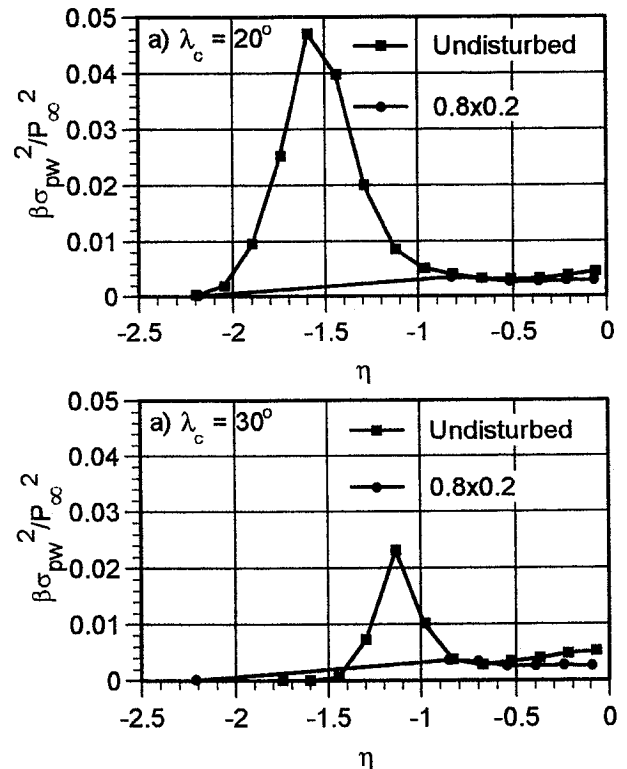
Figure 21: Wall Pressure Variance in the Structural Resonant Frequency Band Upstream of Swept Compression Corners a) $\lambda_c = 20°$, b) $\lambda_c = 30°$

The mechanism by which the loads upstream of the swept corners are reduced is the same as that for the unswept corners. The separation shock is eliminated thus removing the source of low-frequency wall pressure fluctuations upstream of the corner. In the swept interactions, the wall pressure spectra and auto-correlations have the same qualitative behavior as was observed in the unswept interaction. No attempt was made to document the effect of the BLSs on the corner face loads in swept interactions; however, it is expected that the effect would be similar to that in unswept interactions since the mechanisms are the same.

Conclusions

Boundary Layer Separators have been shown to be an effective control technique that can be used to significantly reduce the wall pressure fluctuation energy in the structural resonant frequency band. The BLSs reduce the magnitude of the loads through the interaction and alter their frequency content. These changes come about because the BLSs alter the natural separation and reattachment dynamics. By

using the BLSs, the wall pressure energy in the resonant band is essentially eliminated upstream of the compression corner leading edge and on the corner face it can be reduced by up to 60%.

The BLSs are equally effective in unswept and swept compression corner interactions and can also be used to alter the mean pressure distribution on the compression corner face. The effectiveness of the BLSs in reducing loads on the corner face is dependent on the BLS height and the distance between the BLS and the corner leading edge. Furthermore, it was found that for wedge shaped BLSs, the blunter BLS was more effective in reducing the energy in the structural resonant frequency band despite the separated flow upstream of it. However, using a block-shaped BLS did not reduce the energy in the resonant band further. The present results show that the effectiveness of the BLSs in controlling the loads upstream of the corner is insensitive to the height or placement of the BLS. However, the leading edge angle of the BLS should be less than that needed for incipient separation to avoid a small-scale separated shock wave turbulent boundary layer interaction upstream of the BLS.

References

1. Bogdonoff, S. M., "Some Experimental Studies of the Separation of Supersonic Turbulent Boundary Layers," Heat Transfer and Fluid Mechanics Institute, UCLA, June 23-25, 1955, sec. V, pp. 1-23.
2. Chapman, D. R., D. M. Kuehn, and H. K. Larson, "Investigation of Separated Flows in Supersonic and Subsonic Streams with Emphasis on the Effect of Transition," NACA Report 1356, 1958.
3. Kistler, A. L., "Fluctuating Wall Pressure under a Separated Supersonic Flow," Journal of the Acoustical Society of America, Vol. 36, No. 3, pp. 543-550.
4. Dolling, D. S., "Fluctuating Loads in Shock Wave Turbulent Boundary Layer Interaction: Tutorial and Update," AIAA Paper 93-0284, Jan. 11-14, 1993, Reno, NV.
5. Pozefsky, P., R. D. Blevins, and A. L. Laganelli, "Thermo- Vibro-Acoustic Loads and Fatigue of Hypersonic Flight Vehicle Structures," AFWAL TR-89-3014, Feb. 1989.
6. Raghunathan, S., "Passive Control of Shock Boundary Layer Interaction," Progress in Aerospace Sciences, Vol. 25, No. 3, pp. 271-296, Mar. 1988.
7. Grin, V. T., and N. N. Zakharov, "Experimental Investigation of Effect of Tangential Blowing and Wall Cooling on Flow with Separation," Fluid Dynamics, Vol. 6, pp. 1035-1038, Jun. 1974.
8. Viswanath, P. R., L. Sankaran, P. M. Sagdeo, R. Narasimha, and A. Prabhu, "Injection Slot Location for Boundary Layer Control in Shock-Induced Separation," Journal of Aircraft, Vol. 20, No. 8, pp. 726-732, Aug. 1983.
9. Ball, K. O. W., and R. H. Korkegi, "An Investigation of the Effect of Suction on Hypersonic Laminar Boundary Layer Separation," AIAA Journal, Vol. 6, No. 2, pp. 239-243, Feb. 1968.
10. Viswanath, P. R., "Shock-Wave-Turbulent-Boundary-Layer Interaction and Its Control: A Survey of Recent Developments," Developments in Fluid Mechanics and Space Technology, edited by Narasimha, R., and A. P. J. Abdul Kalam, Indian Academy of Sciences, Bangalore, India, pp. 143-202, 1988.
11. McClure, W. B., "An Experimental Study of the Driving Mechanism and Control of the Unsteady Shock Induced Turbulent Separation in a Mach 5 Compression Corner Flow," Ph.D. Dissertation, Dept. of Aerospace Engineering and Engineering Mechanics, The University of Texas at Austin, Aug. 1992.
12. Kleifges, K. and D. S. Dolling, "Control of Unsteady Shock-Induced Turbulent Boundary Layer Separation Upstream of Blunt Fins," AIAA Paper 93-3281, July 6-9, 1993, Orlando, FL.
13. Barter, J. W., and D. S. Dolling, "Experimental Study of the Use of Vortex Generators to Reduce Fluctuating Pressure Loads in Shock Wave Turbulent Boundary Layer Interactions," AIAA Paper 93-4335, Oct. 25-27, 1993, Long Beach, Ca.
14. Erengil, M. E., and D. S. Dolling, "Physical Causes of Separation Shock Unsteadiness in Shock Wave/Turbulent Boundary-Layer Interactions," AIAA Paper 93-3134, AIAA 24th Fluid Dynamics Conference, July 6-9, 1993, Orlando, FL.

15. Marshall, T., and D. S. Dolling, "Comments on the Computation of Supersonic, Unswept, Turbulent Compression Ramp Interactions," *AIAA Journal*, Vol. 30, No. 8, pp. 2056-2065, Aug. 1992.
16. Gramann, R. A., "Dynamics of Separation and Reattachment in a Mach 5 Unswept Compression Ramp Flow," Ph.D. Dissertation, Dept. of Aerospace Engineering and Engineering Mechanics, The University of Texas at Austin, Dec. 1989.